Geophysical Journal International

Geophys. J. Int. (2013) **194,** 961–978
Advance Access publication 2013 April 30

doi: 10.1093/gji/ggt135

The uppermost mantle shear wave velocity structure of eastern Africa from Rayleigh wave tomography: constraints on rift evolution

J. P. O'Donnell,[1] A. Adams,[2] A. A. Nyblade,[1] G. D. Mulibo[1] and F. Tugume[1]

[1] *Department of Geosciences, The Pennsylvania State University, University Park, PA* 16802*, USA. E-mail: jpo1@psu.edu*
[2] *Department of Earth and Planetary Sciences, Washington University, St. Louis, MO, USA*

Accepted 2013 April 4. Received 2013 April 3; in original form 2012 November 19

SUMMARY

An expanded model of the 3-D shear wave velocity structure of the uppermost mantle beneath eastern Africa has been developed using earthquakes recorded by the AfricaArray East African Seismic Experiment in conjunction with data from permanent stations and previously deployed temporary stations. The combined data set comprises 331 earthquakes recorded on a total of 95 seismic stations spanning Kenya, Uganda, Tanzania, Zambia and Malawi. In this study, data from 149 earthquakes were used to determine fundamental-mode Rayleigh wave phase velocities at periods ranging from 20 to 182 s using the two-plane wave method, and then combined with the similarly processed published measurements and inverted for a 3-D shear wave velocity model of the uppermost mantle. New features in the model include (1) a low-velocity region in western Zambia, (2) a high-velocity region in eastern Zambia, (3) a low-velocity region in eastern Tanzania and (4) low-velocity regions beneath the Lake Malawi rift. When considered in conjunction with mapped seismicity, these results support a secondary western rift branch striking southwestwards from Lake Tanganyika, likely exploiting the relatively weak lithosphere of the southern Kibaran Belt between the Bangweulu Block and the Congo Craton. We estimate a lithospheric thickness of ∼150–200 km for the substantial fast shear wave anomaly imaged in eastern Zambia, which may be a southward subsurface extension of the Bangweulu Block. The low-velocity region in eastern Tanzania suggests that the eastern rift branch trends southeastwards offshore eastern Tanzania coincident with the purported location of the northern margin of the proposed Ruvuma microplate. Pronounced velocity lows along the Lake Malawi rift are found beneath the northern and southern ends of the lake, but not beneath the central portion of the lake.

Key words: Mantle processes; Seismicity and tectonics; Surface waves and free oscillations; Seismic tomography; Dynamics of lithosphere and mantle; Africa.

1 INTRODUCTION

The Cenozoic East African Rift System (EARS), comprising a series of rift zones stretching over 3000 km from the Afar triple junction in the north to beyond the Zambesi River in the south, provides unprecedented access to the entire spectrum of rift development, from the initial stages of continental breakup in eastern Africa to incipient seafloor spreading in Afar (e.g. Prodehl *et al.* 1997; Bastow *et al.* 2011). The rift system is also coincident with, and possibly geodynamically connected to, a pervasive lower mantle low-velocity zone beneath southern Africa rising to at least transition zone depths beneath eastern Africa, known as the African superplume (e.g. Ritsema *et al.* 1999; Nyblade 2011; Hansen *et al.* 2012; Mulibo & Nyblade in press).

In tandem with understanding the influence of mantle processes on the rift system is the question of the role played by pre-existing structures in the localization of rift faulting (e.g. McConnell 1972, 1980; Mohr 1982; Nyblade & Brazier 2002). For example, Ritsema *et al.* (1998) argue that the thick, cold lithospheric keel of the Tanzania Craton exerts a first-order structural control on rift development, with the eastern and western rift branches preferentially located in thinner, warmer mobile belt lithosphere, circumventing the colder, thicker lithosphere of the craton. However, knowledge of possible constraints on rift evolution is limited in the region south of the Tanzania Craton which has not been as extensively studied as more northerly locales. Several seismicity studies have inferred distributary branching of the western rift (e.g. Fairhead & Girdler 1969; Fairhead & Henderson 1977; Foster & Jackson 1998), while Mougenot *et al.* (1986) suggested that the eastern rift trends southeastwards across eastern Tanzania, connecting offshore with the Davie Ridge. By analogy with the bifurcation of the rifts around the Tanzania Craton, this raises the question of whether other geological units or features might be guiding rift propagation, and if so, how?

© The Authors 2013. Published by Oxford University Press on behalf of The Royal Astronomical Society.

Downloaded from https://academic.oup.com/gji/article-abstract/194/2/964/588895 by guest on 25 September 2018

The EARS is also associated geographically with the East African Plateau, which is part of one of the largest topographic anomalies on Earth, the African superswell (Nyblade & Robinson 1994). It has long been debated whether the effects of distinct geodynamic processes have superimposed to produce the geographically contiguous uplifted regions (i.e. eastern Africa, southern Africa and the southern Atlantic Ocean Basin) or whether they are the surface manifestation of the underlying lower mantle African superplume (e.g. Lithgow-Bertelloni & Silver 1998; Gurnis *et al.* 2000).

By extending data coverage into parts of Zambia and eastern Tanzania not well imaged in previously published studies using similar methodologies (Weeraratne *et al.* 2003; Adams *et al.* 2012), we address these issues using an improved and expanded regional-scale tomographic image of the uppermost mantle shear wave velocity structure of eastern Africa. First, the image permits us to track eastern and western rift development beyond the well-studied segments which skirt the flanks of the Tanzania Craton. In doing so, we attempt to ascertain what geological structures might be guiding and facilitating rift evolution. Secondly, in Zambia, the uppermost mantle image affords us the opportunity to examine potential sources for the anomalous topographic uplift away from the major centres of Cenozoic rifting and volcanism which pervade much of eastern Africa.

2 TECTONIC SETTING

The Archean Tanzania Craton forms the nucleus of the Precambrian framework of eastern Africa (Fig. 1). Upon encountering the thick cratonic lithosphere, the Cenozoic EARS bifurcates, with eastern and western branches developing within the succession of Proterozoic mobile belts which skirt the craton. These include the Mezoproterozoic Rwenzori Belt to the north of the craton, the Palaeoproterozoic Ubendian and Usagaran belts to the southwest and southeast of the craton (Fig. 1), respectively, and the Mezoproterozoic Kibaran and Neoproterozoic Mozambique belts to the west and east of the craton, respectively (e.g. Cahen *et al.* 1984). North of the Rwenzori Belt lies the Ugandan Basement Complex (e.g. Leggo 1974).

The eastern rift branch, which developed within the Mozambique Belt, runs south from Ethiopia through west-central Kenya, where it is known locally as the Kenya or Gregory rift, and into northern Tanzania. Rift-related volcanism along the eastern rift branch has progressively migrated southwards, from the earliest volcanic activity in northern Kenya *ca.,* 35–40 Ma (MacDonald *et al.* 2001; Furman *et al.* 2006) to *ca.,* 8 Ma in northern Tanzania (Dawson 1992; Foster *et al.* 1997).

The western rift branch developed within the Rwenzori, Kibaran, Ubendian and Irumide belts, running south and defining the eastern border of the Democratic Republic of Congo (DRC), through southeastern Tanzania and into Malawi. The rift branch includes the Lake Albert, Lake Edward, Lake Kivu, Lake Tanganyika, Lake Rukwa and Lake Malawi rifts. The less volcanic western branch is considered to be significantly younger than the eastern branch, with rifting initiating *ca.,* 12 Ma (e.g. Ebinger 1989; Pasteels *et al.* 1989; Cohen *et al.* 1993; Kampunzu *et al.* 1998). However, Roberts *et al.* (2012) recently suggested that rift initiation in the western branch possibly began more than 14 Myr earlier (*ca.,* 26 Ma), contemporaneously with rifting in Kenya.

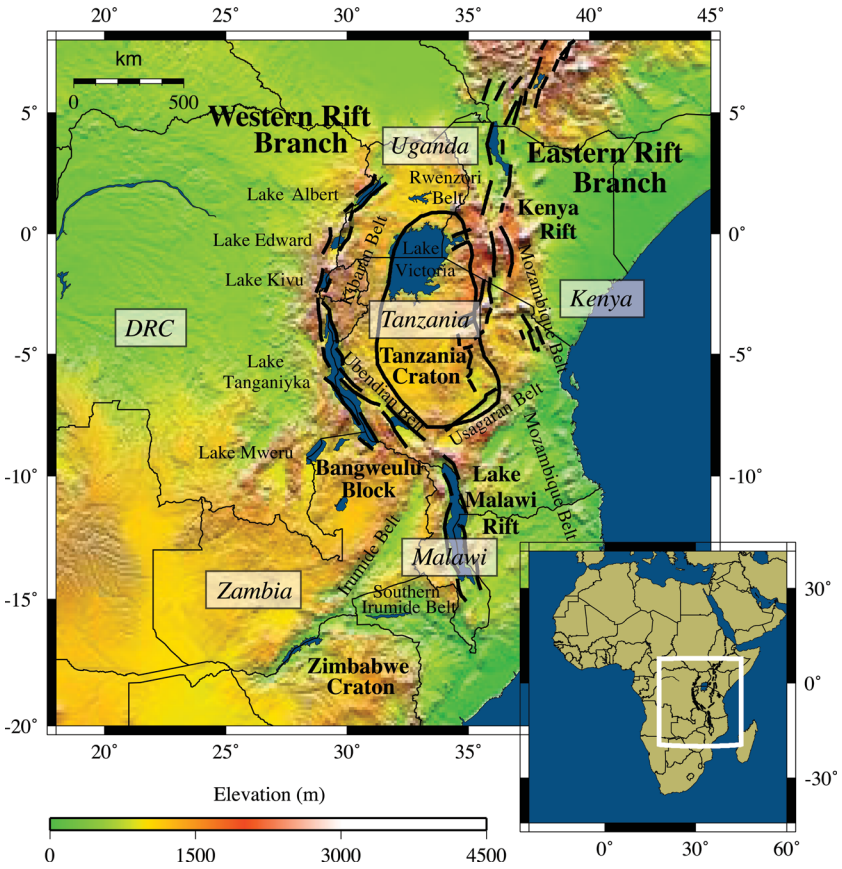


Figure 1. Topographic map of eastern Africa showing geological provinces. Bold lines delineate the Archean Tanzania Craton and major Cenozoic rift faults. Thin lines delineate international borders.

Downloaded from https://academic.oup.com/gji/article-abstract/194/2/961/598895 by guest on 25 September 2018

Southwest of the Ubendian Belt, between the Kibaran Belt in the north and the Irumide Belt to the southeast, is the Bangweulu Block, a cratonic unit underlying most of northern Zambia and adjacent parts of Tanzania and DRC. Based on geochemical analysis, Andersen & Unrug (1984) argue that it is a Palaeoproterozoic structure. However, because the central portion of the Bangweulu Block is covered by Palaeoproterozoic sediments, their measurements were confined to the exposed fringes of the block. Citing whole-rock geochemistry and isotopic data, De Waele *et al.* (2006) argue that, considering its entire lithosphere, the Bangweulu Block is an Archean Craton, as originally proposed by Drysdall *et al.* (1972).

South and east of the Bangweulu Block in eastern Zambia are the Irumide and southern Irumide Belts. U-Th-Pb analyses of zircon indicate that the Irumide Belt is primarily Palaeoproterozoic, but may include some Neoarchean crust (De Waele *et al.* 2009). Based on U-Pb SHRIMP zircon analyses, Johnson *et al.* (2007) showed that the southern Irumide Belt also formed during the Palaeoproterozoic.

2.1 Previous studies

A number of previous authors have examined upper-mantle structure beneath various parts of the study region using both body and surface wave tomography. Using *P*- and *S*-wave traveltime tomography, Ritsema *et al.* (1998) imaged a low-velocity anomaly in the upper mantle beneath the eastern rift branch dipping to the west under the Tanzania Craton and extending to $\geq$400 km depth. They also imaged a region of fast velocities beneath the Tanzania Craton, indicating that the lithospheric keel of the craton extends to a depth of $\sim$200 km. The westward-dipping anomaly was attributed to the flow of a mantle plume around the thick lithospheric keel of the Tanzania Craton by Nyblade *et al.* (2000).

A *P*-wave tomography study of the mantle beneath Kenya by Park & Nyblade (2006) also revealed the presence of a low-velocity anomaly dipping to the west beneath the Tanzania Craton, consistent with earlier tomographic models in Kenya from the KRISP project (Green *et al.* 1991; Achauer & the KRISP Teleseismic Working Group 1994; Achauer & Masson 2002). The limited resolution imposed by the small aperture of the Tanzania and Kenya networks, however, made it difficult for these studies to show conclusively whether the westward-dipping low-velocity anomaly continues at depth beneath the Tanzania Craton connecting to a similar anomaly under the western rift branch.

A study of mantle transition zone discontinuities by Owens *et al.* (2000) using receiver function stacks found evidence for a 30–40 km depression of the 410 km discontinuity, a result that was latter corroborated by Huerta *et al.* (2009) using a larger data set from stations in Tanzania and Kenya. A depressed 410 km discontinuity confirms that the upper-mantle velocity anomaly is largely a thermal structure and that it extends to depths $\geq$410 km. The deep mantle structure under eastern Africa has been further investigated recently using regional and global body wave tomography (Hansen *et al.* 2012; Simmons *et al.* 2012; Mulibo & Nyblade in press). These studies show that the anomalous upper-mantle structure imaged in the above-mentioned studies likely extends through the mantle transition zone and connects with the low-velocity anomaly originating in the lower mantle beneath southern Africa commonly referred to as the African superplume (e.g. Ritsema *et al.* 1999; Gurnis *et al.* 2000).

Using surface wave tomography, Weeraratne *et al.* (2003) also imaged the low-velocity anomaly beneath the eastern rift branch and the Tanzania Craton. A more recent surface wave tomography model from Adams *et al.* (2012), in addition to imaging the low-velocity anomaly under the craton, shows that there are regions of anomalously low velocity beneath the volcanic centres along the western branch of the rift system and that the fast upper-mantle structure under the Tanzania Craton extends to the north beneath the Basement Complex of northern Uganda. Continental-scale surface wave studies show similar results to these regional studies (e.g. Sebai *et al.* 2006; Pasyanos & Nyblade 2007; Priestley *et al.* 2008; Fishwick 2010), although not nearly at the same level of resolution.

Seismic anisotropy has been investigated using body and surface waves. Walker *et al.* (1994) reported inconsistent teleseismic shear wave splitting results beneath the Tanzania Craton and along its southern and southeastern flank, but more consistent splitting elsewhere in the rifts and orogenic belts with the fast polarization directions roughly aligned along strikes. They concluded that anisotropy in Tanzania and Kenya is due to a combination of asthenospheric flow beneath and around the craton, asthenospheric flow from a plume north of central Kenya, fossilized lithospheric anisotropy and aligned magma-filled lenses beneath the rifts.

Bagley & Nyblade (2013) measured shear wave splitting across an expanded network of stations in eastern Africa, noting a preponderance of NE aligned fast polarization directions coupled with local changes around the lithosphere of the Tanzania Craton. From examining the pattern of fast polarization directions along the entire Afro-Arabian rift system, they concluded that the pattern was most readily attributable to mantle flow associated with the African superplume in a generally northerly direction. Using Rayleigh waves, Weeraratne *et al.* (2003) investigated azimuthal anisotropy beneath Tanzania, reporting an average NNW–SSE fast polarization direction, whereas Adams *et al.* (2012) reported generally N–S fast polarization directions beneath an enlarged area of the East African Plateau.

While seismicity studies in eastern Africa have shown the majority of earthquakes to correlate with well-defined rift zones (e.g. Wohlenberg 1969; Fairhead & Girdler 1971; Sykes & Landisman 1974; Båth 1975), Fairhead & Girdler (1969) surmised that three active rift branches might exist in eastern Africa and extend considerably farther south than previously thought: the first extending southwest from the southern end of Lake Tanganyika into northern Botswana, the second extending along the Malawi rift and the third extending along the East African continental margin. Following the work of Fairhead & Girdler (1969), Fairhead & Henderson (1977) mapped two main seismicity branches in Zambia, one striking southwest from the southern end of Lake Tanganyika through Lake Mweru and the border region of Zambia and the DRC, the other striking parallel along the Zambia–Zimbabwe border. In a later seismicity study, Foster & Jackson (1998) surmised that the mapped distribution suggests that the western rift branch possibly bifurcates at the southern end of Lake Tanganyika, lending weight to the previous interpretations.

Although seismicity patterns in northeastern Tanzania delineate the eastern rift branch along the border of the craton (e.g. Mulibo & Nyblade 2009), the pattern in southeastern Tanzania is more diffuse. Båth (1975) mapped seismicity continuing southwards from the Kenya rift through Tanzania and joining the western rift between Lakes Tanganyika and Malawi/Nyasa. Mougenot *et al.* (1986) alternatively suggested that the eastern rift branch may actually trend offshore southeastwards from the Tanzania coastline at 7° south, eventually intercepting the Davie Ridge. A recent studyof seismicity in southeast Tanzania by Mulibo (2012) shows a zone of seismicity trending southeastwards towards the ocean from the southeast

Downloaded from https://academic.oup.com/gji/article-abstract/194/2/961/598895 by guest on 25 September 2018

margin of the Tanzania Craton. He suggested that the seismicity zone might reflect the northern boundary of the proposed Ruvuma microplate (Calais *et al.* 2006; Stamps *et al.* 2008).

3 DATA

The data were amalgamated from several networks and experiments, including the Tanzania Broadband Seismic Experiment (Nyblade *et al.* 1996), the AfricaArray permanent seismic network (africaarray.org), three phases of the AfricaArray East African Seismic Experiment, the southeastern Tanzania Basin Experiment and the Global Seismic Network (GSN, Fig. 2). During phase 1 of the AfricaArray East African Seismic Experiment (2007 August to 2008 December), 20 broad-band seismometers were deployed across Uganda and northwestern Tanzania. This temporary network was subsequently redeployed to southern Tanzania for phase 2 of the experiment between 2008 December and 2010 June. At the end of phase 2, the network was again redeployed to Zambia, where phase 3 data were recorded until 2011 August. The southeastern Tanzania Basin Experiment comprised a network of eight seismometers whose purpose was to elucidate information on the basin structure towards the coast in southeastern Tanzania. This network operated from 2010 February until 2011 July.

We combine the 93 events processed by Weeraratne *et al.* (2003) and the 89 events processed by Adams *et al.* (2012) with 149 new events recorded between 2008 December and 2011 August on phase 2 and 3 stations of the AfricaArray East African Seismic Experiment, the permanent AfricaArray network, four stations of the southeastern Tanzania Basin Experiment and four GSN stations.

Events with magnitudes equal to or greater than 5.5 were sought and sourced in the epicentral distance (Δ) range $30^\circ < \Delta < 120^\circ$. To be considered for analysis, an event had to exhibit high signal-to-noise ratio surface wave waveforms and be recorded at five or more stations. The composite data set includes data from 331 events recorded on 95 seismic stations. Fig. 3 shows the distribution of the earthquakes. Azimuthal coverage is generally very good, although it should be noted that the path coverage does vary with frequency as a result of decreasing signal-to-noise ratios at longer periods and the effects of multipath interference at shorter periods (Fig. 4). However,

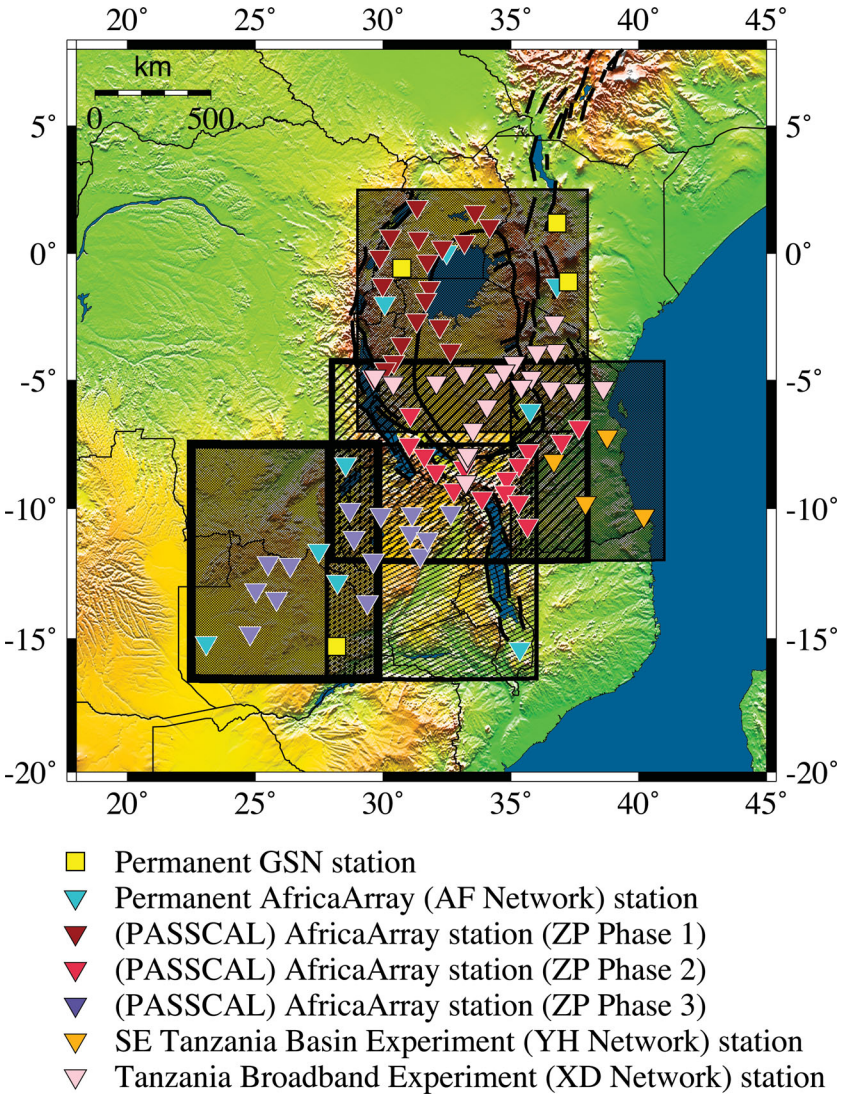


Figure 2. The location of seismic stations used in this study (IRIS network codes are in parentheses in the key). The division of the composite array into five subarrays (displayed rectangles) to minimize array aperture in accordance with the assumptions of two-plane wave tomography are also shown. See Section 4 for details.

Downloaded from https://academic.oup.com/gji/article-abstract/194/2/961/598895 by guest on 25 September 2018

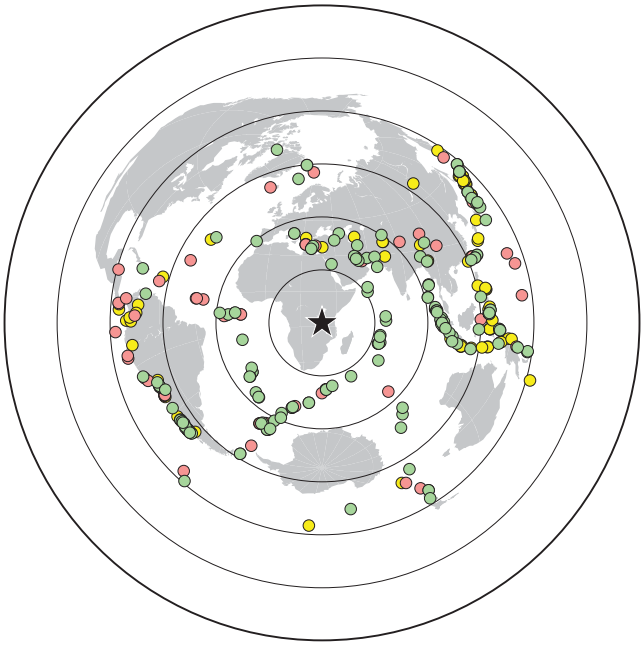


Figure 3. Azimuthal and epicentral distance distribution of the 331 events used in this study. Yellow circles are the 93 events from Weeraratne *et al.* (2003) recorded primarily on the Tanzania Broadband Seismic Experiment network. Red circles are the 89 events from Adams *et al.* (2012) recorded primarily on phase 1 and 2 stations of the AfricaArray East African Seismic Experiment. Green circles are the 149 events recorded primarily on phase 3 stations of the AfricaArray East African Seismic Experiment. Concentric circles are at 30° intervals from the centre of the study area.

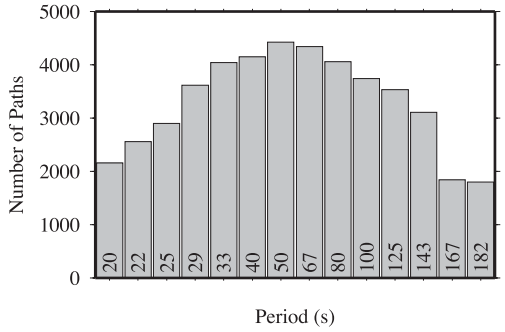


Figure 4. Number of ray paths as a function of period.

the observation and conclusion of Weeraratne *et al.* (2003), that it is largely the density of paths that varies with frequency as opposed to their spatial distribution—meaning that any bias related to the varying coverage should be small or negligible—also holds here (Fig. 5). The likely manifestation of a relatively reduced path density is simply larger model uncertainties due to reduced redundancy in an overdetermined inverse problem.

After normalizing station instrument responses, vertical-component fundamental-mode Rayleigh wave seismograms were analysed across 14 periods ranging from 20 to 182 s. Each Rayleigh wave seismogram was filtered using a narrow bandpass (10 mHz), zero-phase-shift, four-pole Butterworth filter centred at the period of interest (Fig. 6). All filtered seismograms were individually checked and those with poor signal-to-noise ratios discarded. Next, for each period and event, a window was manually selected to isolate the desired Rayleigh waveform from other contaminating seismic phases and/or noise. Upon isolation and extraction, all filtered and windowed seismograms were again individually checked and assessed for quality. Fourier analysis was subsequently employed to determine the phase and amplitude of each remaining seismogram, two pieces of information per seismogram which, following the formulation of Smith & Dahlen (1973), serve as data for the tomographic inversion for azimuthally averaged phase velocities and azimuthal anisotropic coefficients.

4 TWO-PLANE WAVE TOMOGRAPHY

Conventional approaches to surface wave tomography often regard incoming wavefields as single plane waves propagating along great circle paths. However, waveform amplitudes and phases across an array often exhibit effects reminiscent of interference, considered to reflect scattering or multipathing caused by lateral heterogeneities between the source and array. Because a single plane wave is unable to account for such distortions, Forsyth *et al.* (1998) and Forsyth & Li (2005) modelled the incoming wavefield as the superposition

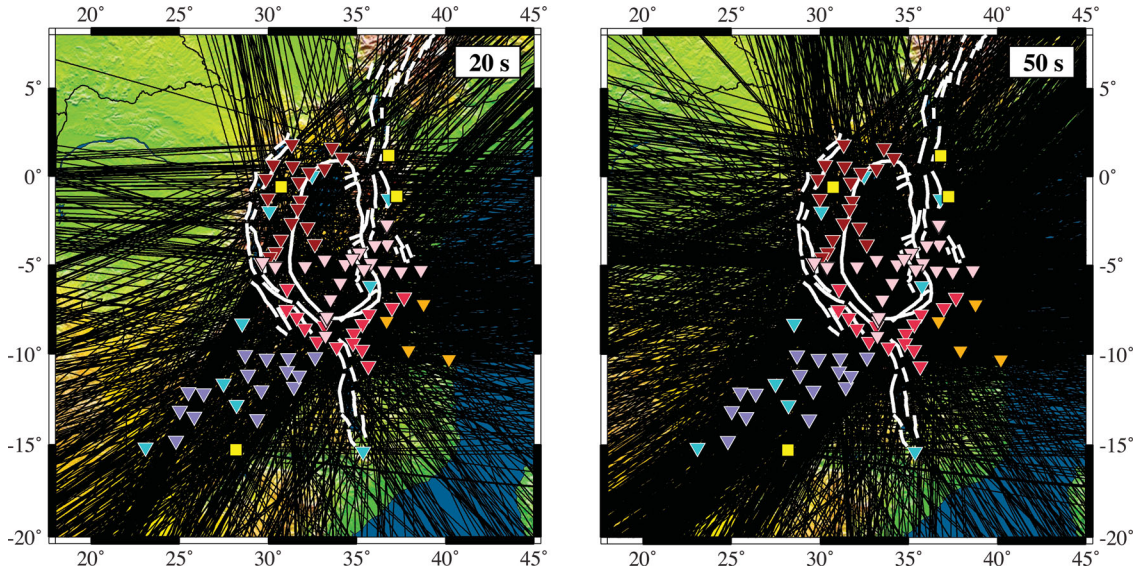


Figure 5. Great circle ray paths at periods 20 and 50 s. Superimposed are the seismic stations as denoted in Fig. 2.

Downloaded from https://academic.oup.com/gji/article-abstract/194/2/961/598895 by guest on 25 September 2018

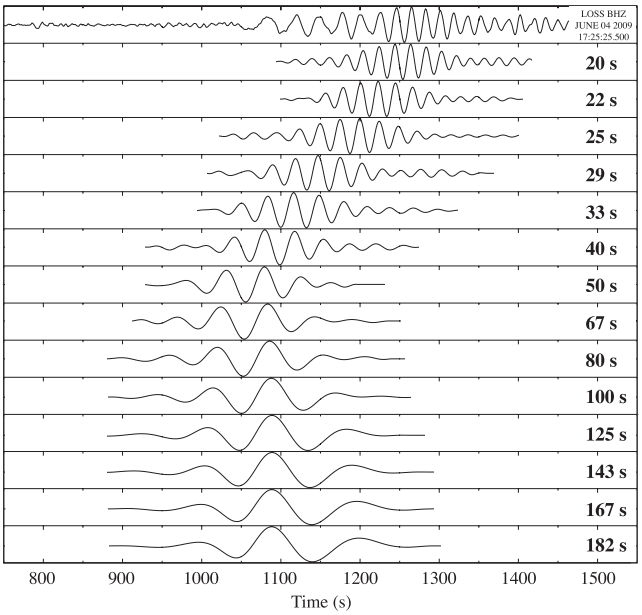


Figure 6. Rayleigh wave dispersion of an event originating in the western Indian Ocean recorded at AfricaArray station LOSS. The raw Rayleigh wave seismogram (top) is filtered into 14 10 mHz wide bands with centre periods ranging from 20 to 182 s and each filtered trace subsequently windowed to isolate the Rayleigh waveform.

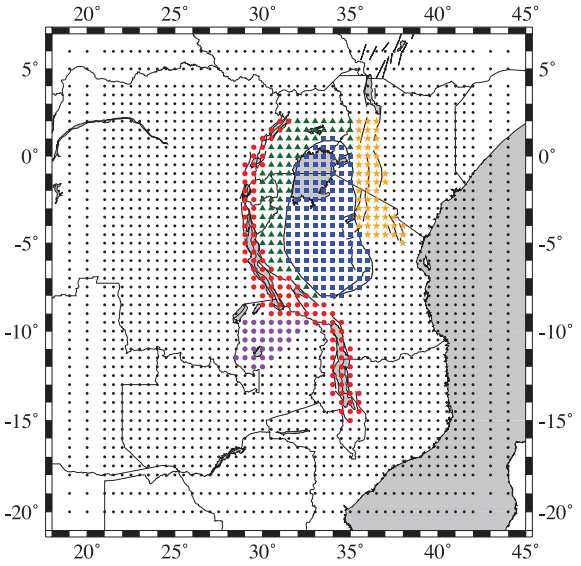


Figure 7. Node locations used in this study. Small black circles represent background nodes. The Bangweulu Block is represented by purple circles, the Western Rift Branch by red circles, the Tanzania Craton by blue squares and the Eastern Rift Branch by orange stars. The area directly north and west of the Tanzania Craton, including parts of the Ruwenzori, Kibaran and Ubendian belts, is designated by green triangles. In total, our grid consists of ∼2300 nodes.

of two interfering plane waves. Li *et al.* (2003) demonstrated that approximating the incoming wavefield thus generally adequately accounts for the aforementioned variations, leading to significant improvements in data fitting and model variance reduction. The two-plane wave method has subsequently been successfully applied in a number of studies in Africa (e.g. Weeraratne *et al.* 2003; Li & Burke 2006; Adams & Nyblade 2011; Li 2011; Adams *et al.* 2012).

Within this approach, the inversion for phase velocities proceeds in two stages: initially, phase velocities are held fixed while the optimum phases, amplitudes and propagation directions of the two modelled incoming plane waves are determined via a simulated annealing method. Next, a linearized least-squares inversion is used to simultaneously determine optimum phase velocities at individual gridpoints and adjusted plane wave parameters (phases, amplitudes and propagation directions) for each event. When the two-plane wave approximation is not a good model for the incoming wavefield, resulting in large data misfits and model parameter variances, that particular event at the period in question is automatically downweighted.

We employ a grid of nodes spaced at 0.5° intervals which spans the area of dense, crossing ray coverage (Fig. 7). Along with starting phase velocity values, phase velocity model parameter damping values are assigned at each node which determine the degree to which the corresponding model parameter may deviate from the initial *a priori* starting model. We found that a damping value of 0.15 km s^{-1} provided a reasonable degree of regularization for stabilization purposes without being overly restrictive. Two exterior rows of nodes spaced at 1° intervals were assigned much relaxed damping values (1.5 km s^{-1}) to preferentially absorb complex wavefield variations that a simple two-plane wave representation is unable to account for.

Being predicated on the assumption of planar wave fronts, the validity of this method is inversely related to the areal extent of the network aperture. Following the approach of Adams *et al.* (2012), we divide the composite array into five more compact subarrays (see Fig. 2). The network divisions are largely naturally determined by the individual network deployments. Where a particular phase of the deployment spanned a large area (e.g. phase 3 of the AfricaArray East African Seismic Experiment), the array associated with that phase was subdivided. It should be borne in mind that the temporal overlap of the three phases was minimal relative to their deployment periods.

Initially, we inverted for an average 1-D phase velocity curve representing the entire study area. The inversion consistently converged to the same solution for a selection of starting models based both on the previous results from Weeraratne *et al.* (2003) and Adams *et al.* (2012) and on standard earth models. We next utilized this average curve as a starting model to invert for an average curve for each of the geological regions denoted in Fig. 7. The curve obtained for a particular region then served as a starting model for phase velocity inversions at all nodes within that region.

For the first series of inversions, the aim of which was to produce a cascade of progressively more accurate starting models for the ultimate 2-D inversion, a Gaussian sensitivity function was employed to account for structure off the great circle path. We assessed various widths for the Gaussian influence zone around the ray path, ranging between extremes of 25 and 500 km. A scale length in the vicinity of 100 km offered a best compromise between the unduly rough models arising from overfitting data at the shortest length scales and the suppressive-fit, laterally diluted models at the longest length scales. However, finite frequency effects, which become important when trying to image structure on the scale of a wavelength, cannot be fully accounted for by this approach. Yang & Forsyth (2006a,b) adapted and applied finite frequency sensitivity kernels developed by Zhou *et al.* (2004) to surface wave tomographic problems, demonstrating improved resolution of smaller scale structures compared with inversions which used a Gaussian-shaped influence zone around the ray paths. Li (2011) subsequently showed that finite frequency effects are most significant at periods greater than 100 s. Following the method of Yang & Forsyth (2006a,b), we calculated

Downloaded from https://academic.oup.com/gji/article-abstract/194/2/961/598895 by guest on 25 September 2018

and applied finite frequency sensitivity kernels in the subsequent final inversion for azimuthally averaged phase velocities and azimuthal anisotropy coefficients.

5 PHASE VELOCITIES

Fig. 8 (and corresponding Table 1) shows the result of the inversion for the regional average phase velocity curve. Superimposed for comparison are similarly derived average curves for east Africa (Adams *et al.* 2012) and for southern Africa (Adams & Nyblade 2011). Fig. 8 shows that the phase velocities obtained agree well with those determined by Adams *et al.* (2012). Velocities are slightly lower at periods less than 50 s and slightly higher at periods above 50 s, although largely within error bounds. As noted by Adams *et al.* (2012), the comparable phase velocities at periods of less than 30 s for eastern and southern Africa may be indicative of similar crustal structure. However, at periods above 30 s the curves for eastern and southern Africa diverge significantly, suggesting distinct upper-mantle structure.

Fig. 9 (and corresponding Table 1) shows average phase velocity curves for each of the regions outlined in Fig. 7. Again, the average curve for southern Africa is superimposed for comparison. The Tanzania Craton and west-of-craton region phase velocities are comparable to average southern Africa velocities at periods up to 33 s, but at longer periods the southern Africa velocities are significantly higher. Below 33 s, the other regions exhibit phase velocities to varying degrees lower than southern Africa velocities, while the same marked divergence occurs at periods above this. The western rift branch is significantly slower than all other geological regions at shorter periods, although at most periods above 67 s the eastern rift branch is slowest, a finding similarly observed by Adams *et al.* (2012). At periods up to 67 s the Tanzania Craton is the fastest region, followed by the west-of-craton region and the Bangweulu Block. However, the west-of-craton region is the fastest region at periods beyond 67 s and the Bangweulu Block is faster than the Tanzania Craton at periods between 100 and 167 s. Between 50 and 80 s, the Tanzania Craton phase velocity profile is almost flat and increases only gradually between 80 and 120 s. Similarly, the profiles for the eastern rift and background regions, on average, increase only slightly between 50 and 100 s.

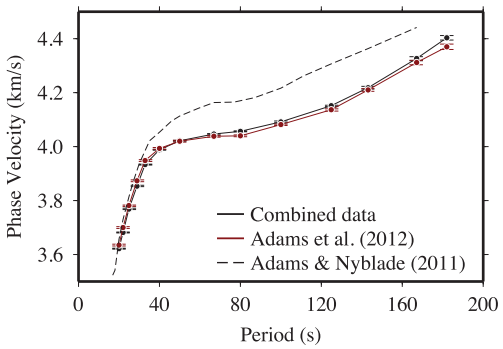


Figure 8. The average 1-D phase velocity dispersion curve for the entire study area (black). The average 1-D curves determined by Adams *et al.* (2012) for East Africa (red) and by Adams & Nyblade (2011) for southern Africa (dashed) are shown for comparison. Error bars indicate one standard deviation. The numerical values are listed in Table 1.

Employing these curves as regional starting models, we inverted for 2-D phase velocity structure. In this case, we utilize covariance and resolution matrices to mask model regions exhibiting the greatest variance and poorest resolution. Fig. 10 shows the model uncertainty, calculated from the covariance matrix, at a selection of periods. Model variance is least in the centre of the study area as expected, where the majority of seismic stations are located and path crossing is maximal, and decreases towards the peripheries. Superimposed on model variance fluctuations between periods resulting from differing path coverage is a natural variance increase due to the fact that a given phase error will translate to a larger error in time with increasing period.

We graphically represent the resolution matrix in terms of conventional 2° and 3° square harmonically alternating ±5 per cent checkerboard anomalies (Fig. 11). Due to the spatial correspondence between areas of low model uncertainty and high resolution, we employ the uncertainty maps to define threshold uncertainty values at each period above which map areas are masked. Threshold values range from a minimum of 0.04 km s^{-1} at 20 s to a maximum of 0.06 km s^{-1} at 182 s. Due to the high density of crossing paths, checkerboards are generally very well resolved, particularly in northern and central regions where smearing is minimal and amplitude recovery is typically 60 per cent or better. Because of a diminution in path crossing towards the southeast and southwest, smearing becomes more apparent causing amplitude recovery to dip below 50 per cent. Due to the increasing wavelengths, 2° checkers could not be resolved at 167 and 182 s. However, 3° anomalies were recovered, albeit in relatively more confined areas.

Fig. 12 shows the corresponding phase velocity maps. At periods up to 100 s, the Tanzania Craton is a relatively fast feature, particularly evident at shorter periods. As Adams *et al.* (2012) similarly observed, the region bordering the craton to the west and north

Table 1. Average phase velocity values for each of the designated areas in Fig. 7. Standard deviations are in brackets.

Period (s)	Average	Background	Western rift	West of craton	Tanzania Craton	Eastern rift	Bangweulu Block
20	3.622(0.002)	3.617(0.003)	3.477(0.007)	3.683(0.007)	3.654(0.003)	3.618(0.009)	3.562(0.008)
22	3.682(0.002)	3.677(0.003)	3.536(0.006)	3.728(0.006)	3.734(0.003)	3.691(0.009)	3.680(0.009)
25	3.769(0.002)	3.751(0.003)	3.621(0.007)	3.811(0.006)	3.812(0.003)	3.719(0.008)	3.764(0.008)
29	3.854(0.002)	3.825(0.003)	3.682(0.008)	3.890(0.006)	3.910(0.003)	3.831(0.008)	3.846(0.008)
33	3.933(0.002)	3.896(0.003)	3.780(0.007)	3.970(0.006)	3.990(0.003)	3.886(0.008)	3.930(0.008)
40	3.988(0.002)	3.966(0.003)	3.850(0.008)	4.033(0.006)	4.031(0.003)	3.915(0.008)	3.980(0.008)
50	4.022(0.002)	4.011(0.004)	3.936(0.008)	4.023(0.007)	4.071(0.004)	3.962(0.008)	3.995(0.008)
67	4.046(0.002)	4.030(0.004)	3.965(0.009)	4.080(0.007)	4.083(0.004)	3.945(0.009)	3.983(0.010)
80	4.057(0.002)	4.049(0.005)	3.994(0.011)	4.106(0.009)	4.078(0.005)	3.998(0.010)	4.051(0.012)
100	4.092(0.003)	4.074(0.006)	4.065(0.011)	4.136(0.009)	4.102(0.005)	4.021(0.011)	4.117(0.014)
125	4.151(0.003)	4.155(0.007)	4.139(0.014)	4.217(0.012)	4.134(0.006)	4.118(0.013)	4.172(0.020)
143	4.218(0.005)	4.255(0.009)	4.186(0.018)	4.246(0.016)	4.211(0.008)	4.144(0.015)	4.229(0.024)
167	4.326(0.007)	4.354(0.013)	4.234(0.024)	4.360(0.021)	4.323(0.011)	4.281(0.024)	4.300(0.030)
182	4.403(0.008)	4.417(0.016)	4.334(0.031)	4.436(0.026)	4.408(0.014)	4.353(0.031)	4.341(0.035)

Downloaded from https://academic.oup.com/gji/article-abstract/194/2/961/598895 by guest on 25 September 2018

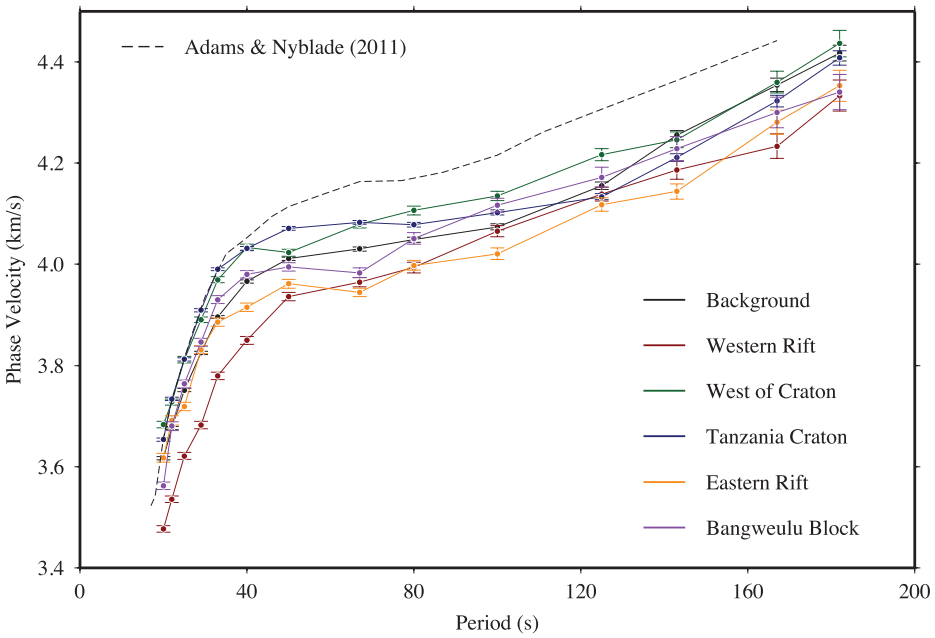


Figure 9. Average phase velocity dispersion curves for each of the designated areas in Fig. 7. The average 1-D curve for southern Africa (dashed) from Adams & Nyblade (2011) is shown for comparison. Error bars are one standard deviation. The numerical values are listed in Table 1.

exhibits velocities comparable to the craton interior at most periods. In the newly expanded study area to the south, notable fast anomalies are apparent in the vicinity of and to the south of the Bangweulu Block at all periods, and in northern Mozambique at periods greater than 100 s. At shorter periods, the lowest velocities are concentrated below the Kenya rift, Kivu rift, Lake Rukwa rift and Malawi rift, coincident with Quaternary to recent volcanism. This morphology generally persists with increasing period, although becoming more diffuse. In addition to the low velocities which generally delineate the eastern and western rift branches and the Malawi rift, velocity lows in the newly expanded study area are apparent in western Zambia and trending offshore eastern Tanzania. Actual phase velocity magnitudes are broadly similar to those reported by Adams *et al.* (2012).

Fig. 13 shows the average azimuthal anisotropy for periods up to 143 s. The general trend is a transition from NWW–SEE oriented fast directions at shorter periods to NW–SE/NNW–SSE oriented fast directions at longer periods. In the vicinity of an active rift zone, observed anisotropy might reflect fossil anisotropy preserved in the lithosphere from past tectonic activity, aligned magmatic cracks in the mantle, mantle flow or a combination thereof (e.g. Gao *et al.* 1997). Given that the fast direction of anisotropy resulting from aligned magmatic cracks would be expected to be parallel to a rift axis (∼ N–S in this case, e.g. Gao *et al.* 1997; Kendall *et al.* 2005), the observed average azimuthal anisotropy at the shortest periods most plausibly reflects the superposition of various preserved structural trends, for example, NWW–SEE for the Tanzania Craton, W–E for the Rwenzori Belt, NE–SW for the Kibaran Belt, NW–SE for the Ubendian Belt, W–E for the Usagaran Belt, N–S for the Mozambique Belt, NWW–SEE for the Bangweulu Block and NE–SW for the Irumide Belt (e.g. Cahen *et al.* 1984; Shackelton 1986; Lenoir *et al.* 1994). At periods greater than 67 s, the average fast direction is more NW–SE/NNW–SSE oriented, probably indicating an increased influence of the generally N–S trending rifts which broaden with increasing depth. The preservation of fossil anisotropy in the mantle in the vicinity of the rifts is unlikely given that the mobility of olivine crystals is increased at the associated elevated temperatures (Vinnik *et al.* 1992; Gao *et al.* 1997). The average fast direction at 125 s, W–E, is somewhat anomalous in that it deviates from the general NW–SE trend evident at the other longer periods. That said, a W–E oriented anisotropic trend is not inconsistent with the structural trends outlined above. However, given the consistent transition in fast directions across the other periods, we conservatively prefer not to interpret this result.

Although our results are broadly consistent with Adams *et al.* (2012) at periods up to 67 s, the average fast directions reported by Adams *et al.* (2012) exhibit more internal variability between periods and deviate considerably from our results for periods 80 to 143 s. The stable transition in average fast directions between periods now apparent is likely the result of bolstering seismic resolution by almost doubling the data set relative to the Adams *et al.* (2012) study. Other deviations, such as those at the longest periods, are not unexpected given that the study area over which the anisotropy is being averaged is now significantly larger.

Anisotropy magnitudes show a slight increase with period, apart from at 143 s, where it decreases. However, given the error bounds, such a conclusion is tenuous. Conservatively, we conclude only that the percentage peak-to-peak anisotropy is less than ∼1 per cent at all periods. Azimuthal anisotropy is poorly constrained at periods 167 and 182 s and thus not included in Fig. 13 or discussed.

6 SHEAR WAVE VELOCITY STRUCTURE

At each node location, a phase velocity dispersion curve with standard deviations was extracted from the 2-D phase velocity and uncertainty maps, respectively, and inverted for a 1-D shear wave velocity profile. Taking slices through the suite of 1-D profiles allows us to build 2-D shear wave velocity maps. Park *et al.* (2008), Adams & Nyblade (2011) and Adams *et al.* (2012) adopted the same approach.

The shear wave velocity inversion algorithm was developed by Julià *et al.* (2000) to jointly invert phase and/or group velocities with receiver functions. As a linearized inversion, a starting model

Downloaded from https://academic.oup.com/gji/article-abstract/194/2/961/598895 by guest on 25 September 2018

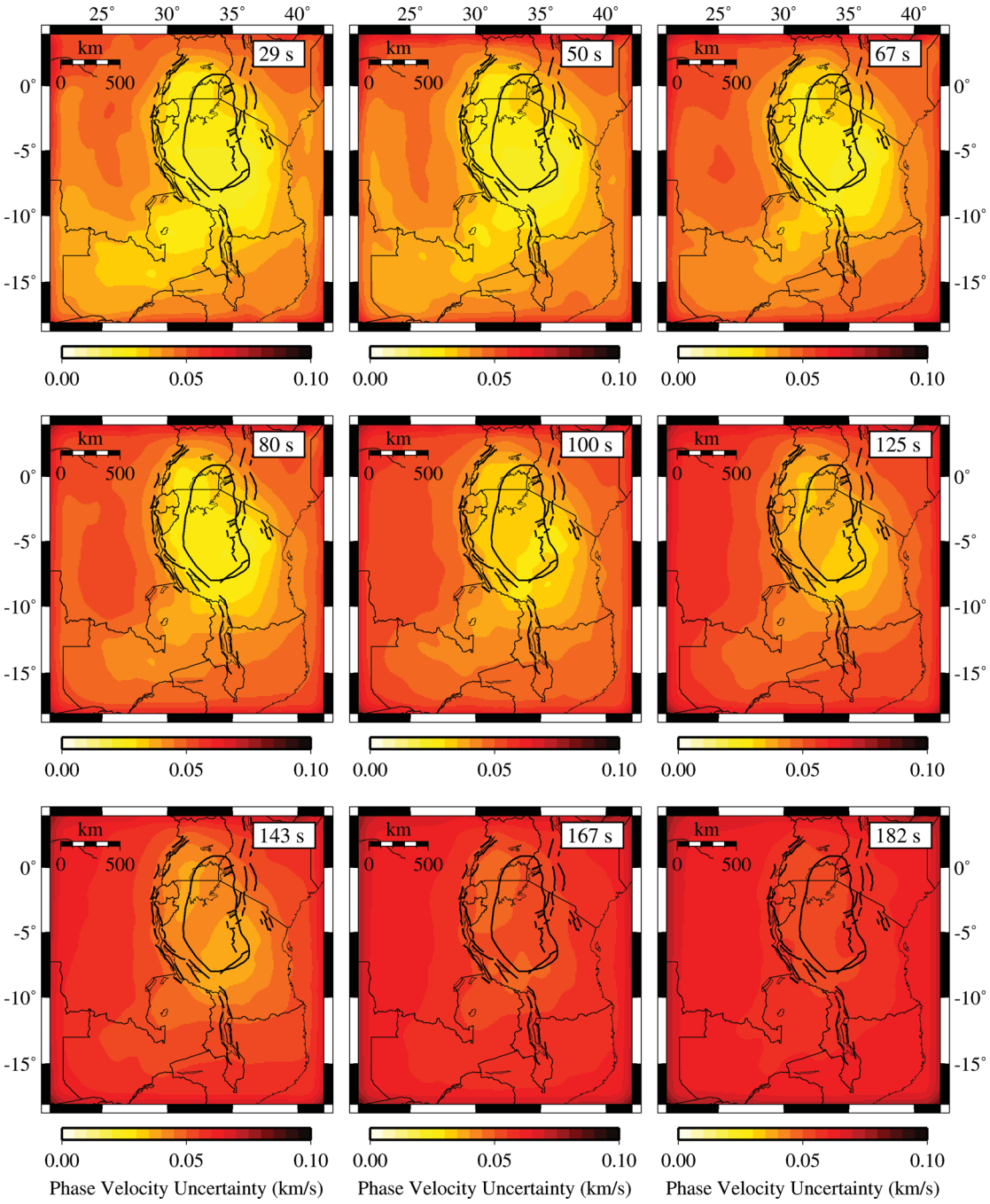


Figure 10. Model uncertainty from the 2-D inversion for a range of periods.

must be furnished and regularization, in this case in the form of smoothing and damping, is necessary to stabilize the inversion. In this study, the shear wave model is constrained using only the phase velocity measurements.

Crustal structure was initialized in each of the geological areas using the parametrization of Adams *et al.* (2012) (Table 2). Relative to the mantle, the crustal portion of the model is confined to the neighbourhood of initial values due to the fact that (i) good average crustal constraints generally exist (Tugume *et al.* 2012, and references therein) and (ii) our surface wave data only significantly sample the lowermost crust at the very shortest periods. We expect the vast majority of phase velocity variations to reflect upper-mantle structure and thus permit more expansive model space exploration, through no damping, at those depths. For the results presented here, the Moho discontinuity was modelled via a 1-km thick layer fixed at the estimated Moho depths across which large steps in velocity structure were permitted by relaxing the smoothing constraint. By modelling different kinds of Moho (discontinuities versus gradational), we determined that the corresponding upper-mantle shear wave velocity profiles only differed in the ∼20 km immediately below the Moho. Beyond this, they converged to the same solution. Consequently, we present and interpret uppermost mantle shear wave velocity structure only for depths equal to and greater than 68 km. To avoid large, physically implausible contrasts between adjacent layers, uniform vertical smoothing was applied to the upper-mantle portion of the model (Fig. 14),

Downloaded from https://academic.oup.com/gji/article-abstract/194/2/961/598895 by guest on 25 September 2018

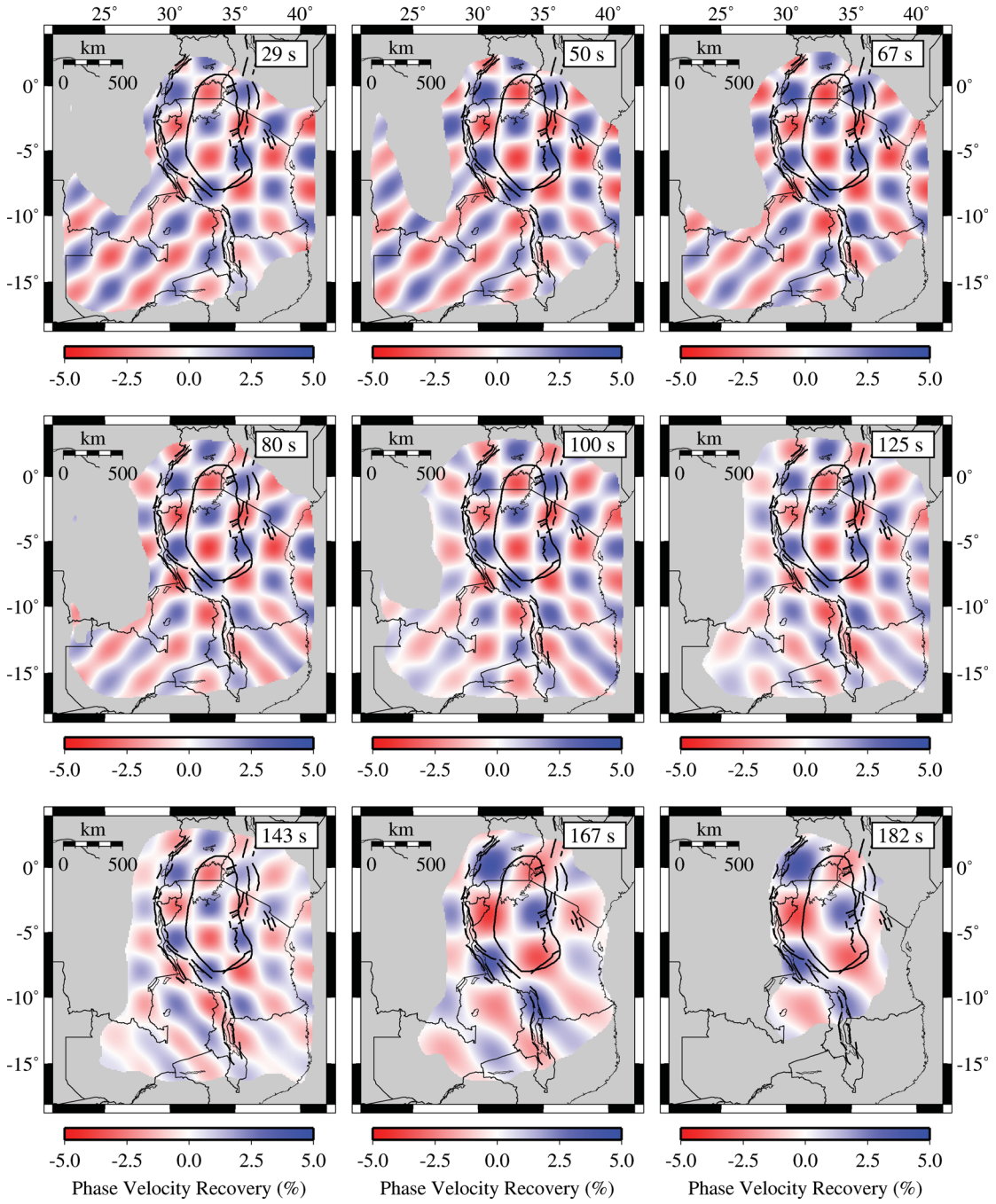


Figure 11. Model resolution of the 2-D inversion. Input ±5 per cent anomalies were 2° squares for periods up to 143 s and 3° squares for periods 167 and 182 s. Regions of lower model certainty according to Fig. 10 are masked.

parametrized in 6 km thick layers to a depth of 250 km, and 10 km thereafter.

Fig. 14 illustrates both the necessity of smoothing regularization and the choice of an appropriate value via a suite of phase velocity dispersion inversions for the average shear wave velocity structure of the Tanzania Craton. At very low (or no) smoothing, unstable and physically unrealistic shear wave profiles are obtained to match the data to a high degree. Conversely, overly strong smoothing leads to suppressed shear wave profiles which cannot explain the data adequately (Fig. 14). A smoothing value which represents a compromise between both extremes is desirable, returning a minimum structure model which also contains stable higher frequency features and fits the data well. In our case, stable, consistent minimum structure profiles emerge for smoothing values between ∼10 and 100, from which we selected a value of 30 as optimally fulfilling the sought criteria. Fig. 15 shows the average shear wave profile of the Tanzania Craton for the range of smoothing values between 10 and 100, from which uncertainty bounds can be estimated. The shear velocity uncertainty is generally less than ∼0.15 km s^{-1} above 200 km depth, increasing to ∼0.25 km s^{-1} for depths below that. These uncertainty bounds are largely consistent across the suite of nodal 1-D shear wave velocity inversions.

In an analogous manner to the phase velocity inversion, a succession of starting models was generated to be employed in

Downloaded from https://academic.oup.com/gji/article-abstract/194/2/961/598895 by guest on 25 September 2018

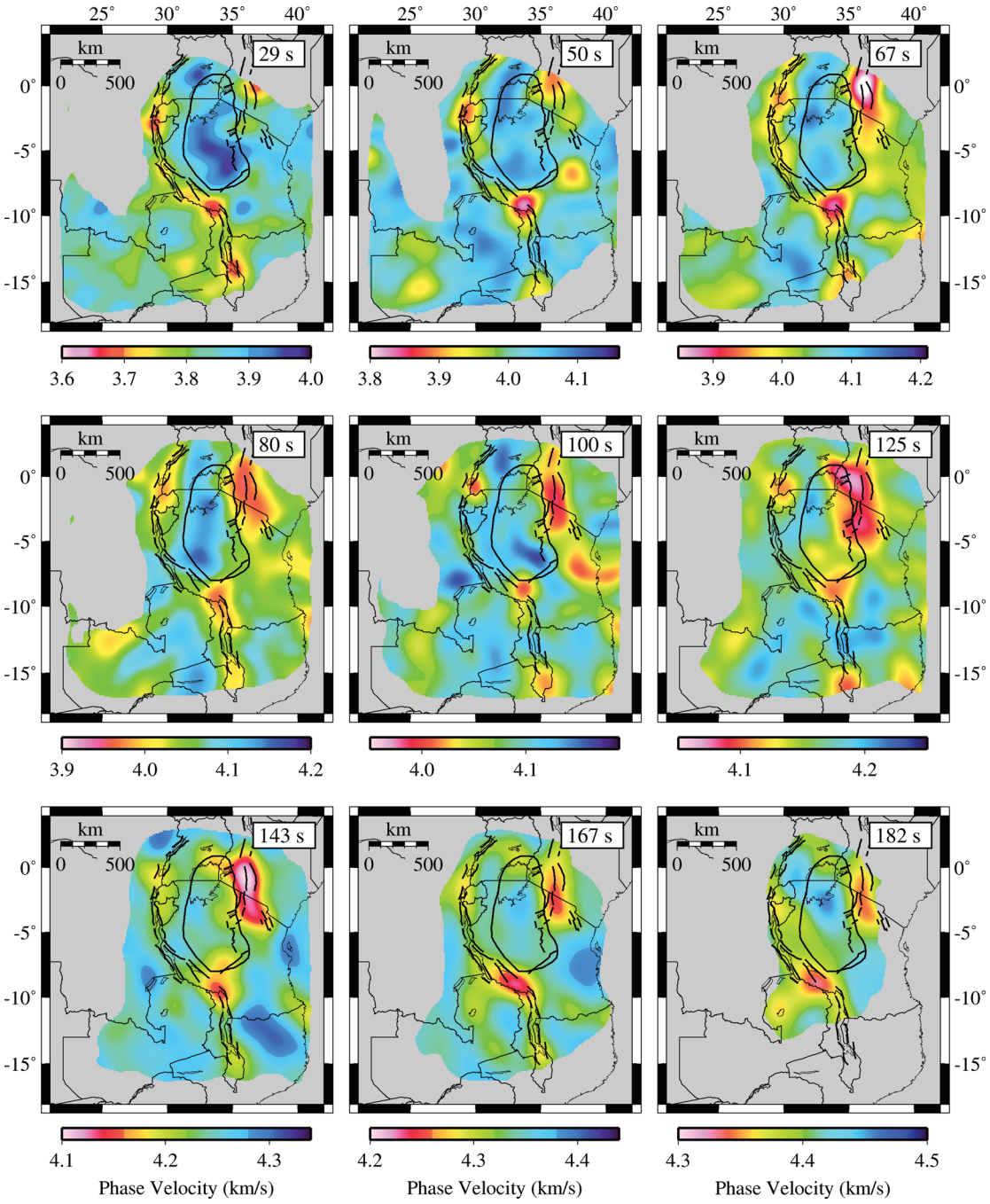


Figure 12. Phase velocity maps from the 2-D inversion at a range of periods. Regions of lower model certainty and resolution are masked.

consecutive inversions. Regional shear wave starting models were obtained by inverting the regional average phase velocity dispersion curves (Fig. 9) from initial shear wave models based on the aforementioned crustal models above an IASP91 (Kennett & Engdahl 1991) upper mantle. The resulting regional shear wave profiles were subsequently employed as starting models for the respective nodes within each geological region.

As the peak sensitivity of Rayleigh waves to shear wave structure occurs at a depth approximately equal to one-third of the wavelength (e.g. Weeraratne *et al.* 2003), we do not expect our longest period waves to have encoded a significant amount of transition zone information. Furthermore, because the azimuthal anisotropy is not well constrained at 167 and 182 s, a significant trade-off may exist between it and the azimuthally averaged phase velocity which together comprise the azimuthally anisotropic phase velocity (Smith & Dahlen 1973). Consequently, we constrained the shear wave profiles to converge on IASP91 velocities at the 410 km discontinuity, thus mapping all structural variations into the upper mantle. However, we estimate that tapering the shear wave profiles smoothly towards the 410 km discontinuity influences structure to approximately 100–150 km above the discontinuity, and thus conservatively we do not interpret 2-D shear wave maps below 220 km depth. We refer the reader to Adams *et al.* (2012) for further discussion about structure below 220 km depth.

Fig. 16 shows slices through the shear wave model at a selection of depths. At upper-mantle depths of less than 100 km, the

Downloaded from https://academic.oup.com/gji/article-abstract/194/2/961/598895 by guest on 25 September 2018

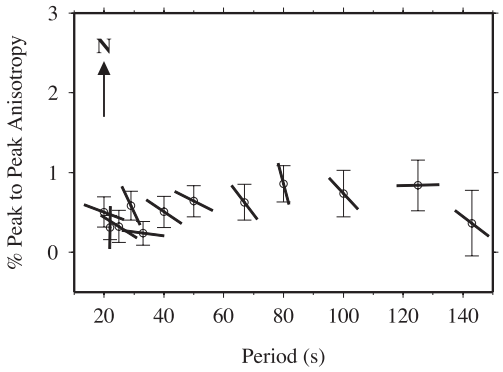


Figure 13. Orientation of fast polarization directions and percentage peak-to-peak azimuthal anisotropy as a function of period. Error bars are one standard error at each period.

Tanzania Craton and Bangweulu Block are prominent fast features exhibiting velocities in the vicinity of 4.65–4.7 km s^{-1}. Comparable velocities extend beyond the craton boundary to the north beneath the Rwenzori Belt and the Ugandan Basement Complex and to the west beneath the Ubendian and Kibaran belts, while slightly reduced velocities extend eastwards beneath northeastern Tanzania. It is noteworthy that the southern and northern portions of the craton are markedly distinct at 60 km depth, with the southern half exhibiting significantly faster velocities.

Between 100 and 160 km, an anomaly in eastern Zambia south of the geographical location of the Bangweulu Block emerges as the dominant fast feature, with a magnitude in the vicinity of 4.7 km s^{-1}. Over the same depth range, a progressive westward migration of the fast velocities associated with the Tanzania craton is apparent.

At depths of less than 120 km, low wave speeds with magnitudes between 4.2 and 4.4 km s^{-1} are concentrated beneath the Quaternary to recent volcanics spatially coincident with the Kenya rift, the Lake Kivu rift and the Rungwe Volcanic Province, while encompassing diffuse low-velocity zones more broadly delineate both rift branches. A notable exception is a low-velocity zone in western Zambia.

At depths greater than about 140 km, a dominant slow feature is found beneath the eastern rift branch, exhibiting velocities as low as 4.2 km s^{-1}. Interestingly, a low-velocity zone trending offshore eastern Tanzania is apparent at these depths, as well as the low-velocity region in western Zambia. Apart from a localized anomaly east of the Lake Edward and Kivu rifts, the western rift branch does not exhibit comparable slow velocities at these depths.

7 DISCUSSION

While our findings are naturally linked to the work of Weeraratne *et al.* (2003) and Adams *et al.* (2012), the fact that data added in this study comprise over 80 per cent of the total allows us to credibly critique correlations between the models.

At 68 and 80 km depth, the Tanzania Craton dominates, representing the aforementioned nucleus of the East African tectonic framework. The extension of fast velocities to the west and north beyond the margin of the craton, previously noted by Adams *et al.* (2012), is apparent. They suggested that this might reflect the adjacent fold belts overthrusting the craton. We also image the eastward extension of fast velocities from the craton into the Mozambique Belt in northeastern Tanzania, consistent with similarly elevated lithospheric mantle velocities measured beneath the Mozambique Belt by Brazier *et al.* (2000). Having imaged the same feature, Adams *et al.* (2012) concluded that the Tanzania Craton likely extends eastwards at depth beneath the Mozambique Belt in northern and central Tanzania, consistent with geochemical studies which similarly invoke a model of two distinct but overlapping lithospheric mantles in this locality (Fritz *et al.* 2009; Mana *et al.* 2012). Additional fast velocity anomalies imaged at depths of 68 and 80 km coincide with the geographical location of the Bangweulu Block and, albeit at the model periphery where resolution degrades, the northern terminus of the Zimbabwe Craton. Focused low velocities are associated with the major Quaternary volcanic centres on both rift branches at these depths. It is interesting to note that elevated velocities are also apparent along sections of the western rift branch away from the volcanic centres, including parts of the Lake Malawi rift. This is also apparent in the tomographic models produced by Adams *et al.* (2012) and Mulibo & Nyblade (in press).

A number of salient features emerge or become apparent at deeper mantle depths. First is the progressive westward migration with depth of fast velocities associated with the Tanzania Craton. This phenomenon has been remarked upon by Adams *et al.* (2012) and Mulibo & Nyblade (in press), both of whom attributed it to the erosion of the cratonic keel in the east by an impinging plume-related thermal anomaly associated with the widely imaged westward-dipping low-velocity structure beneath the eastern rift (e.g. Ritsema *et al.* 1998; Park & Nyblade 2006). Many investigators have argued that this structure is probably connected to the African superplume (e.g. Benoit *et al.* 2006; Park & Nyblade 2006; Huerta *et al.* 2009; Adams *et al.* 2012; Hansen *et al.* 2012; Mulibo & Nyblade in press).

Following Weeraratne *et al.* (2003), we estimate a representative value of ∼140–160 km for the thickness of the lithosphere beneath the Tanzania Craton based on the depth to the maximum negative velocity gradient in the average shear wave velocity profile for the entire craton (Fig. 15). This value is consistent with thicknesses reported by Adams *et al.* (2012, 150–200 km), Fishwick (2010, ∼150–160 km), Pasyanos & Nyblade (2007, 150–200 km) and Weeraratne *et al.* (2003, ∼170 km), but contrasts with the value of 225–250 km reported by Priestley *et al.* (2008).

The model mode and eastern rift velocities at 200 km depth are ∼2.5 and ∼5 per cent slower than IASP91, respectively. Adopting the conversion factor of 1 K for a velocity perturbation of

Table 2. Crustal starting models for the shear wave inversions. The thickness (km) and corresponding shear wave velocity (km s^{-1}) in parentheses are shown for each crustal layer.

Geological area	Moho depth	Layer 1	Layer 2	Layer 3	Layer 4	Layer 5
Background	38	2 (3.00)	15 (3.45)	10 (4.00)	11 (4.00)	–
Western Rift	45	2 (2.55)	15 (3.50)	15 (3.79)	13 (3.79)	–
West of Craton	40	2 (3.00)	09 (3.70)	09 (3.70)	10 (3.90)	10 (3.90)
Tanzania Craton	40	2 (3.00)	09 (3.70)	09 (3.70)	10 (3.90)	10 (3.90)
Eastern Rift	35	2 (2.55)	12 (3.50)	10 (3.79)	11 (3.79)	–
Bangweulu Block	38	2 (2.00)	15 (3.45)	10 (4.00)	11 (4.00)	–

Downloaded from https://academic.oup.com/gji/article-abstract/194/2/961/598895 by guest on 25 September 2018

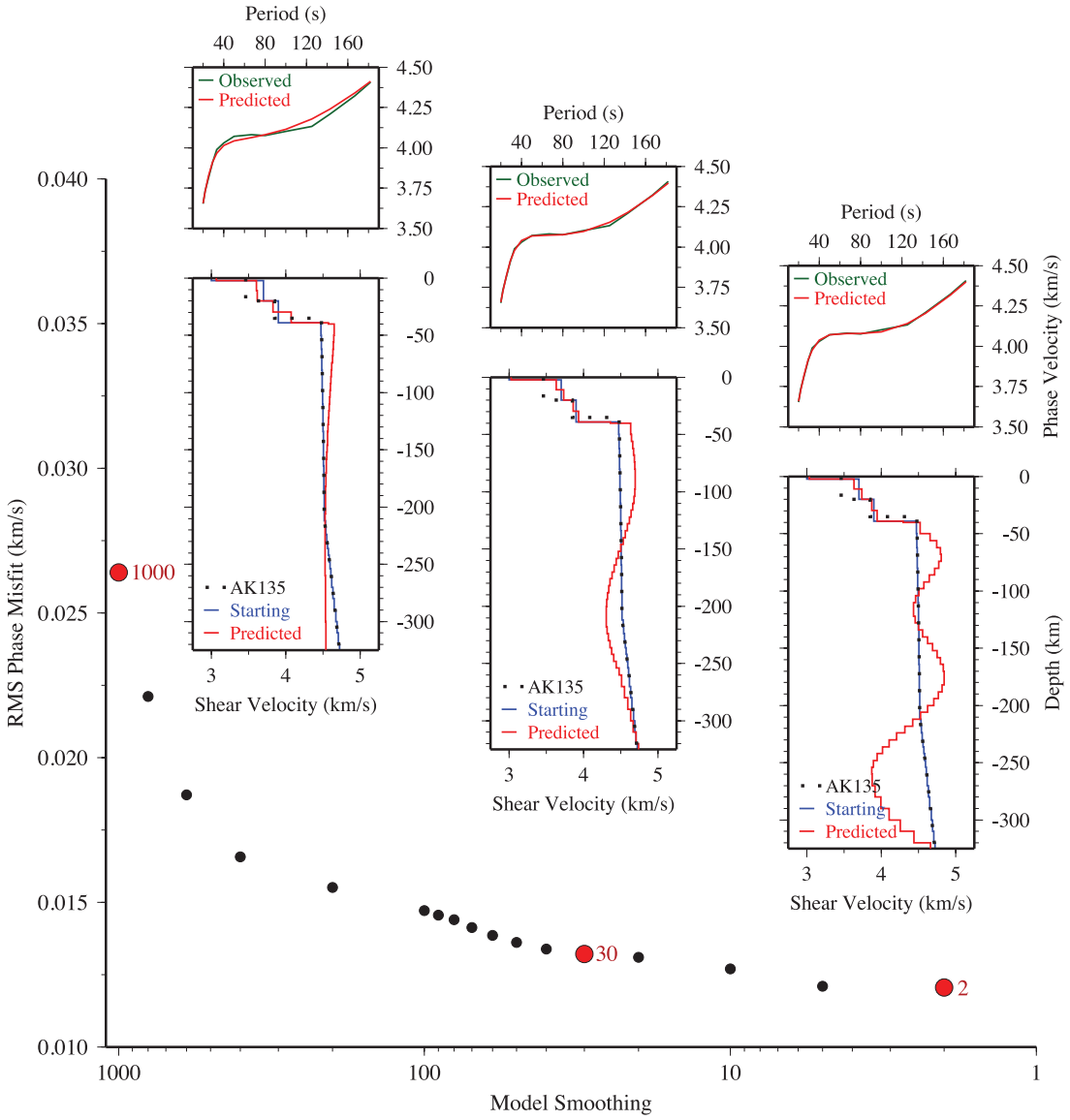


Figure 14. Trade-off between model smoothness and data fitting. Each point represents an average shear wave profile for the Tanzania Craton derived using a particular smoothing value. Oversmoothing (left-hand panels) suppresses structure resulting in poor data fitting, whereas insufficient smoothing (right-hand panels) results in unstable, unrealistic structure explaining the data. Optimal smoothing (middle panels) provides good data fitting through a stable, minimum structure model. The shear wave maps shown in Fig. 16 were derived employing the intermediate smoothing value (30) shown.

0.0012 km s^{-1} (Faul & Jackson 2005; Wiens *et al.* 2008) employed by Adams *et al.* (2012) for comparison, the model mode and eastern rift velocity differentials relative to IASP91 would translate to thermal anomalies of ∼100 and ∼200 K, respectively. However, it must be borne in mind that the regularization imposed over the course of both inversions for phase and shear wave velocities almost certainly results in an underestimation of velocity anomaly magnitudes. Furthermore, a bijective mapping from velocity to thermal anomalies is likely a gross oversimplification given that a multitude of factors including composition, grain size, partial melt, water content and anisotropy affect seismic velocities (e.g. Sobolev *et al.* 1996; Karato & Karki 2001). The conversion is further complicated by the fact that disparities exist among investigators in quantifying both the magnitudes and relative influences of the various sensitivities. For example, while temperature is often considered the principal cause of upper-mantle heterogeneity (e.g. Goes *et al.* 2000), others argue that composition can play a substantial role (e.g. Deschamps *et al.* 2002; Artemieva *et al.* 2004). Adams *et al.* (2012) acknowledged the limitations of the simplistic velocity-to-thermal anomaly translation in explaining the unrealistically large 415 K temperature perturbation converted from their shear wave model minimum at 300 km depth. Indeed Rooney *et al.* (2012) concluded from a geochemical analysis of 53 primitive magmas throughout East Africa that the regional slow-velocity anomalies cannot be attributed entirely to elevated mantle temperatures. They argued that CO_2 assisted melt production in the African superplume is a contributor to the slow seismic velocities and reported a modest regional maximum temperature anomaly of 140 K above ambient mantle in Djibouti.

Acknowledging both the limitations of a direct translation from velocity to thermal anomalies and the modelled underestimation of velocity anomaly magnitudes, our estimate of a ∼200 K thermal anomaly at 200 km depth beneath the eastern rift is reasonably consistent with projected thermal anomaly magnitudes at the top of the transition zone beneath the eastern rift branch based on receiver

Downloaded from https://academic.oup.com/gji/article-abstract/194/2/961/598895 by guest on 25 September 2018

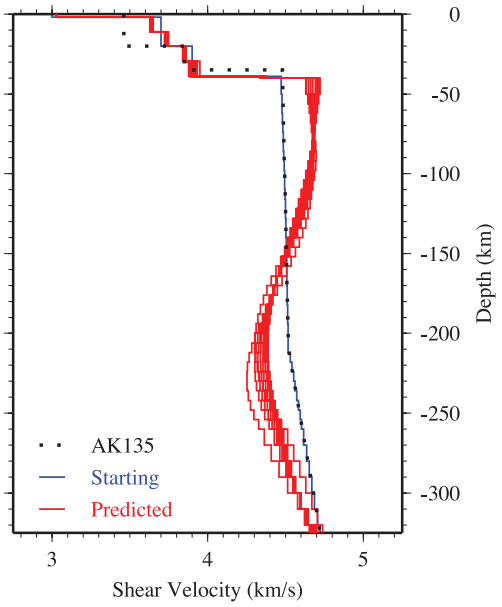


Figure 15. Variability in the average shear wave profile for the Tanzania Craton for a range of plausible smoothing values. The shear velocity uncertainty is generally less than ~0.15 km s^{-1} above 200 km depth, increasing to ~0.25 km s^{-1} below that.

functions (200–300 and 350 K respectively; Owens *et al.* 2000; Huerta *et al.* 2009), attenuation analysis (140–280 K; Venkataraman *et al.* 2004) and the aforementioned more broad scope geochemical study for East Africa ($\leq$ 140 K; Rooney *et al.* 2012).

Given that many studies have investigated the potential link between the pervasive mantle low-velocity anomaly underlying the East African Plateau and the African superplume, we instead focus the remainder of our discussion on uppermost mantle structure and rift development.

At model slices between 100 and 160 km depth, an anomaly in eastern Zambia south of the Bangweulu Block emerges as the dominant fast feature, with a magnitude in the vicinity of 4.7 km s^{-1}. Although the Irumide Belt is reported to include some Archean crust (De Waele *et al.* 2009), the southern Irumide Belt, with which the fast anomaly coincides most geographically, is regarded as a Palaeoproterozoic belt (Johnson *et al.* 2007). In the absence of additional information, we tentatively suggest that the fast structure might represent the southward subsurface extension of the Bangweulu Block. Using the metric of the average depth to the maximum negative velocity gradient in the corresponding shear wave velocity profiles, we estimate a lithospheric thickness of ~150–200 km for the structure. Although not as well constrained, this value exceeds the estimated thickness of the lithosphere beneath the Tanzania Craton (~140–160 km). The fact that the proposed southward subsurface extension of the Bangweulu Block exhibits velocities and a lithospheric thickness comparable to the Tanzania Craton is consistent with the interpretation of the Bangweulu Block as an Archean Craton (Drysdall *et al.* 1972; De Waele *et al.* 2006).

It is widely accepted that the main rift system bifurcates initially in the north to circumvent the Tanzania Craton. However, numerous seismicity studies have postulated the existence of distributary branches of the western rift (Fig. 17). In particular, as reviewed in Section 2.1, it has been suggested that a subbranch trends southwestwards from Lake Tanganyika through Lake Mweru and into northern Botswana (e.g. Fairhead & Girdler 1969, 1971), with Foster & Jackson (1998) suggesting that bifurcation occurs at the southern end of Lake Tanganyika. Meanwhile, Fairhead & Henderson (1977) charted an additional seismicity zone further south along the Zambia–Zimbabwe border striking parallel to the aforementioned subbranch. They postulated that Precambrian structures associated with the southern and northern margins of the Congo and Zimbabwe cratons exert a governing influence on the seismicity trends.

Although towards the model periphery, when analysed in conjunction with the mapped seismicity (Fig. 17), the low-velocity structures imaged in southern DRC and western Zambia support the contention of distributary western rift subbranching. Mulibo & Nyblade (in press) imaged similarly trending spatially coincident relative low-velocity zones in Zambia. In addition to suggested developmental constraints imposed by the Congo and Zimbabwe cratons, we believe that the fast structure imaged in eastern Zambia, regardless of its provenance, exerts a controlling influence on western rift branch propagation: the proposed secondary rift branch strikes southwestwards from Lake Tanganyika, likely exploiting the relatively weak lithosphere of the southern Kibaran Belt between the Bangweulu Block and Congo Craton by analogy with the preceding bifurcation further north of the rift system around the Tanzania Craton. The known and accepted western rift branch forges southeastwards through the Ubendian Belt separating the Tanzania Craton and Bangweulu Block, thereafter turning south. The fact that the velocity lows associated with the proposed secondary western rift branch are only substantially pronounced at the deepest model slices is suggestive of nascent rifting.

Given that the uppermost mantle beneath much of northern Zambia is not perturbed, we conclude that the origin for the anomalous topography across northern Zambia must reside at deeper mantle depths. The African superplume, inferred to rise to at least transition zone depths beneath northern Zambia (e.g. Hansen *et al.* 2012; Mulibo & Nyblade in press), is a feasible candidate.

Turning to the eastern rift branch, our model, particularly the low-velocity regions seen at depths of 158 and 182 km, supports the suggestion by Mougenot *et al.* (1986) that the eastern rift branch trends offshore southeastwards from eastern Tanzania at ~7° south. This trend has recently been supported by a seismicity study in southeast Tanzania by Mulibo (2012) which mapped a zone of seismicity extending southeastwards towards the ocean from the southeastern margin of the Tanzania Craton. That study confirmed a similar although somewhat sparser pattern already evident from events in the International Seismological Centre (ISC) catalogue (Fig. 17). Although our model does not preclude the possibility that another branch may be developing southwestwards from the southeast corner of the craton as suggested by Bàth (1975), it does indicate that the branch trending to the southeast is dominant. This raises the question of what might be governing rift development along the eastern branch. Mulibo (2012) suggested that the seismicity pattern might be associated with the northern boundary of the proposed Ruvuma microplate (Calais *et al.* 2006; Stamps *et al.* 2008). However, a southward adjustment of the purported location of the northern margin of the microplate was required to coincide with the mapped seismicity zone (Mulibo 2012). While the corresponding low-velocity zone imaged here is somewhat diffuse, a reasonably compelling correlation with the northern Ruvuma microplate boundary as proposed by Calais *et al.* (2006) and Stamps *et al.* (2008) is apparent, particularly at 158 km depth (Fig. 17). At the same depth, the southeastward trending seismicity zone mapped by Mulibo (2012) abuts the southern edge of the diffuse low-velocity zone we associate with the offshore bearing eastern rift branch.

Downloaded from https://academic.oup.com/gji/article-abstract/194/2/961/598895 by guest on 25 September 2018

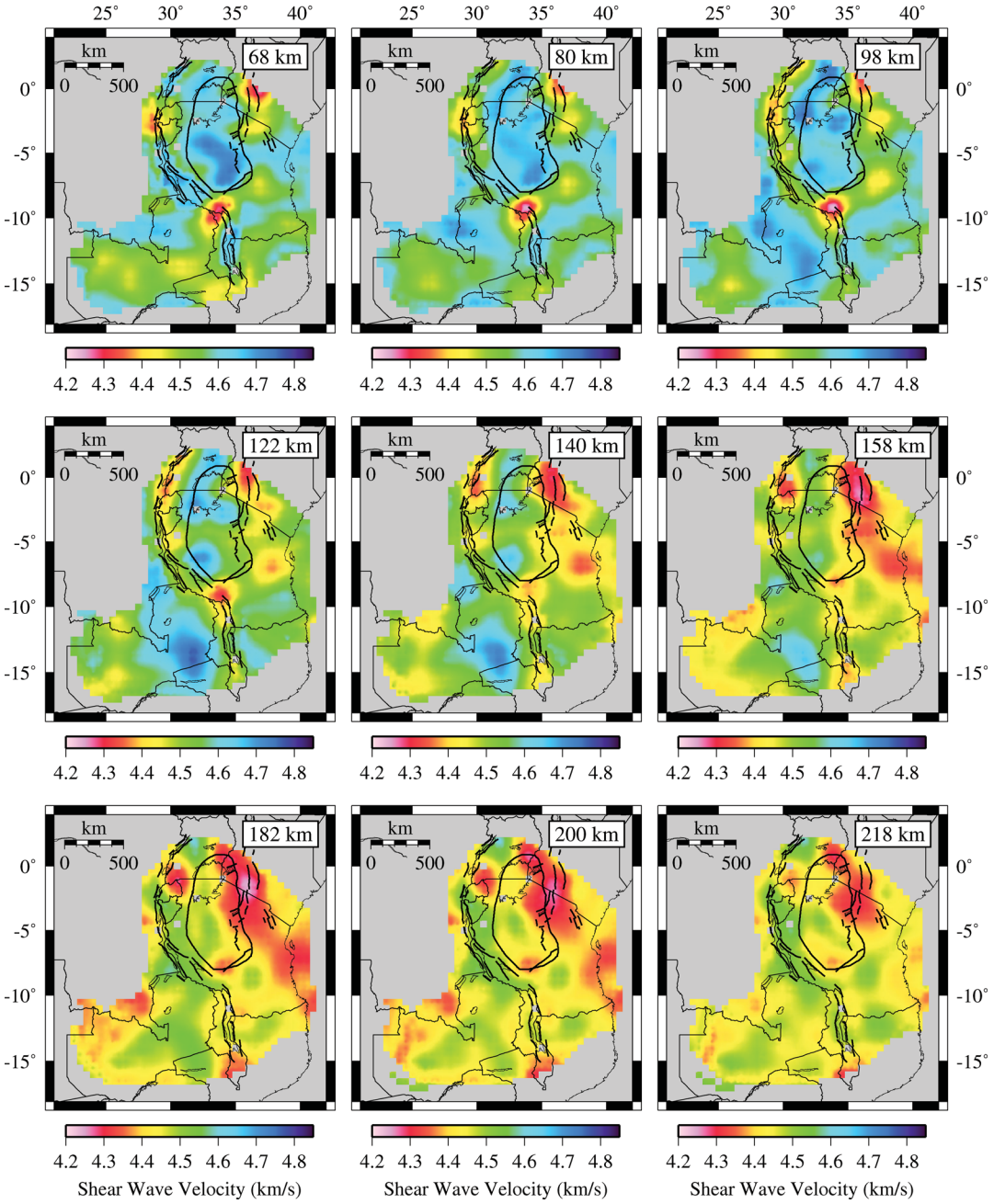


Figure 16. Shear velocity maps at a selection of depths. Shear velocity profiles were extracted only at nodes for which at least eight phase velocity dispersion measurements were available. All other node locations are masked.

8 CONCLUSION

In this study, fundamental-mode Rayleigh wave phase velocities at periods spanning 20–182 s were determined using the two-plane wave tomography method of Forsyth & Li (2005) based on data from 331 teleseismic earthquakes recorded primarily on AfricaArray East African stations. As expected, higher phase velocities are associated with the Tanzania Craton while lower phase velocities delineate the eastern and western rift branches. Average azimuthal anisotropy exhibits a general transition from NWW–SEE oriented fast directions at shorter periods to NW–SE/NNW–SSE oriented fast directions at longer periods, largely in line with previous determinations. At the shortest periods, the observed anisotropy most plausibly reflects the superposition of various preserved geological structural trends, whereas at periods greater than 67 s, the average fast direction probably indicates an increased influence of the generally N–S trending rifts which broaden with increasing depth.

The phase velocities were inverted for a quasi-3-D shear wave velocity model of the uppermost mantle underlying eastern Africa. At lithospheric mantle depths less than 80 km, the Tanzania Craton and Bangweulu Block are prominent fast features, while focused low-velocity anomalies are concentrated beneath the major Quaternary volcanic centres in both rift branches. We estimate that the lithospheric keel of the Tanzania Craton extends to ∼140–160 km depth on average, consistent with previous investigations. With increasing depth, diffuse low velocities more broadly delineate the main rift branches.

Downloaded from https://academic.oup.com/gji/article-abstract/194/2/961/598895 by guest on 25 September 2018

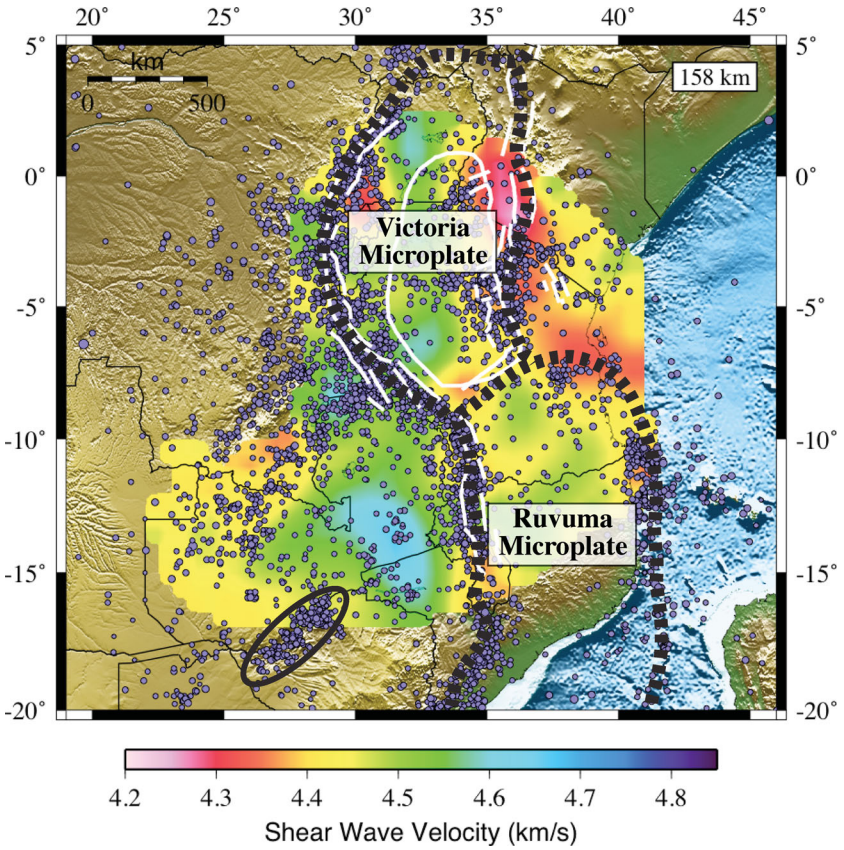


Figure 17. Eastern Africa seismicity 1966–present (magnitudes > 3.2) from the ISC catalogue superimposed on the shear wave velocity model 158 km depth slice. The proposed Ruvuma and Victoria microplate boundaries from Stamps *et al.* (2008) are outlined. The ellipse in the southwest delineates induced seismicity associated with the Kariba Lake Dam.

New features in the model include (1) a low-velocity region in western Zambia, (2) a high-velocity region in eastern Zambia, (3) a low-velocity region in eastern Tanzania and (4) low-velocity regions beneath the Lake Malawi rift. The low-velocity zone imaged in western Zambia is supportive of a previously inferred nascent rift branch extending to the southwest of southern Lake Tanganiyka. This rift branch likely exploits the relatively weak lithosphere of the southern Kibaran Belt between the Bangweulu Block and the Congo Craton. At depths exceeding ∼100 km, an anomaly in eastern Zambia emerges as a dominant fast structure with an associated estimated lithospheric thickness of ∼150–200 km. This structure is possibly the subsurface southward extension of the Bangweulu Block. The fact that the velocity and lithospheric thickness of the body are comparable to those of the Tanzania Craton is consistent with the interpretation of the Bangweulu Block as an Archean Craton. By analogy with the bifurcation of the rift system around the Tanzania Craton, and considering the distribution of seismicity in Zambia, it is likely that this structure, whatever its provenance, has exerted considerable influence on the nascent development of the western rift branch. The low-velocity zone in eastern Tanzania suggests that the eastern rift branch trends southeastwards offshore eastern Tanzania at a location coincident with the purported northern border of the proposed Ruvuma microplate, a determination consistent with mapped seismicity in eastern Tanzania. Pronounced velocity lows along the Lake Malawi rift are found beneath the northern and southern ends of Lake Malawi/Nyasa, but not beneath the central portion of the lake. Elevated velocities are also apparent along sections of the western rift branch away from the volcanic centres.

The fact that the uppermost mantle beneath much of northern Zambia is not perturbed points to a deeper mantle origin for the anomalous topography found across northern Zambia, potentially the African superplume.

ACKNOWLEDGEMENTS

This study was funded by National Science Foundation grants OISE-0530062, EAR-0440032 and EAR-0824781. We would like to thank Incorporated Research Institutions for Seismology (IRIS)-PASSCAL, the Tanzania Geological Survey, the University of Dar es Salaam, the Uganda Geological Survey, the Zambia Geological Survey, Penn State University and many individuals from those institutions for their assistance with fieldwork. Waveform data were obtained from the IRIS Data Management Center (IRIS-DMC). Constructive reviews from Graham Stuart and Steve Gao greatly improved the focus of this paper. Figures were produced using the Generic Mapping Tools (GMT) software package of Wessel & Smith (1998).

REFERENCES

Achauer, U. & Masson, F., 2002. Seismic tomography of continental rifts revisited: from relative to absolute heterogeneities, *Tectonophysics,* **358** (1–4), 17–37.

Achauer, U. & the KRISP Teleseismic Working Group, 1994. New ideas on the Kenya rift based on the inversion of the combined dataset of the 1985 and 1989/90 seismic tomography experiments, *Tectonophysics,* **236**(1–4), 305–329.

Downloaded from https://academic.oup.com/gji/article-abstract/194/2/961/598895 by guest on 25 September 2018

Adams, A. & Nyblade, A., 2011. Shear wave velocity structure of the southern African upper mantle with implications for the uplift of southern Africa, *Geophys. J. Int.,* **186**(2), 808–824.

Adams, A., Nyblade, A. & Weeraratne, D., 2012. Upper mantle shear wave velocity structure beneath the East African plateau: evidence for a deep, plateauwide low velocity anomaly, *Geophys. J. Int.,* **189**(1), 123–142.

Andersen, L.S. & Unrug, R., 1984. Geodynamic evolution of the Bangweulu Block, northern Zambia, *Precambrian Res.,* **25**(1–3), 187–212.

Artemieva, I.M., Billien, M., Leveque, J.J. & Mooney, W.D., 2004. Shear wave velocity, seismic attenuation, and thermal structure of the continental upper mantle, *Geophys. J. Int.,* **157,** 607–628.

Bagley, B. & Nyblade, A.A., 2013. Seismic anisotropy in eastern Africa, mantle flow, and the African superplume, *Geophys. Res. Lett.,* doi:10.1002/grl.50315.

Bastow, I.D., Keir, D. & Daly, E., 2011. The Ethiopia Afar Geoscientific Lithospheric Experiment (EAGLE): probing the transition from continental rifting to incipient seafloor spreading, in *Volcanism and Evolution of the African Lithosphere,* pp. 51–76, eds Beccaluva, L., Bianchini, G. & Wilson, M., Geological Society of America Special Paper 478.

Båth, M., 1975. Seismicity of the Tanzania region, *Tectonophysics,* **27**(4), 353–379.

Benoit, M.H., Nyblade, A.A. & VanDecar, J.C., 2006. Upper mantle P-wave speed variations beneath Ethiopia and the origin of the Afar hotspot, *Geology,* **34,** 329–332.

Brazier, R.A., Nyblade, A.A. & Langston, C.A., 2000. Pn wave velocities beneath the Tanzania Craton and adjacent rifted mobile belts, East Africa, *Geophys. Res. Lett.,* **27**(16), 2365–2368.

Cahen, L., Snelling, N.J., Delhal, J. & Vail, J.R., 1984. *The Geochronology and Evolution of Africa,* Oxford Univ. Press, New York.

Calais, E., Hartnady, C., Ebinger, C. & Nocquet, J.M., 2006. Kinematics of the East African Rift from GPS and earthquake slip vector data, in *Structure and Evolution of the Rift Systems within the Afar Volcanic Province, Northeast Africa,* Vol. 259, pp. 9–22, eds Yirgu, G., Ebinger, C.J. & Maguire, P.K.H., Geological Society of London Special Publications.

Cohen, A.S., Soreghan, M.J. & Scholz, C.A., 1993. Estimating the age of formation of lakes: an example from Lake Tanganyika, East African Rift system, *Geology,* **21,** 511–514.

Dawson, J., 1992. Neogene tectonics and volcanicity in the North Tanzania sector of the Gregory Rift Valley: contrasts with the Kenya sector, *Tectonophysics,* **204,** 81–92.

De Waele, B., Liégeois, J.P., Nemchin, A.A. & Tembo, F., 2006. Isotopic and geochemical evidence of proterozoic episodic crustal reworking within the Irumide Belt of south-central Africa, the southern metacratonic boundary of an Archaean Bangweulu Craton, *Precambrian Res.,* **148**(3–4), 225–256.

De Waele, B., Fitzsimons, I.C.W., Wingate, M.T.D., Tembo, F., Mapani, B. & Belousova, E.A., 2009. The geochronological framework of the Irumide Belt: a prolonged crustal history along the margin of the Bangweulu Craton, *Am. J. Sci.,* **309**(2), 132–187.

Deschamps, F., Trampert, J. & Snieder, R., 2002. Anomalies of temperature and iron in the uppermost mantle inferred from gravity data and tomographic models, *Phys. Earth planet. Inter.,* **129,** 245–264.

Drysdall, A.R., Johnson, R.L., Moore, T.A. & Thieme, J.G., 1972. Outline of the geology of Zambia, *Geol. Mijnbouw,* **51,** 265–276.

Ebinger, C.J., 1989. Tectonic development of the western branch of the East African rift system, *Geol. soc. Am. Bull.,* **101,** 788–791.

Fairhead, J.D. & Girdler, R.W., 1969. How far does the rift system extend through Africa? *Nature,* **221,** 1018–1020.

Fairhead, J.D. & Girdler, R.W., 1971. The seismicity of Africa, **24,** 271–301.

Fairhead, J.D. & Henderson, N.B., 1977. The seismicity of southern Africa and incipient rifting, *Tectonophysics,* **41**(4), T19–T26.

Faul, U.H. & Jackson, I., 2005. The seismological signature of temperature and grain size variations in the upper mantle, *Earth planet. Sci. Lett.,* **234,** 119–134.

Fishwick, S., 2010. Surface wave tomography: imaging of the lithosphere-asthenosphere boundary beneath central and southern Africa? *Lithos,* **120**(1–2), 63–73.

Forsyth, D.W. & Li, A., 2005. Array analysis of two-dimensional variations in surface wave phase velocity and azimuthal anisotropy in the presence of multipathing interference, in *Seismic Earth: Array Analysis of Broadband Seismograms,* pp. 81–97, eds Levander, A. & Nolet, G., American Geophysical Union, Washington, DC.

Forsyth, D.W., Webb, S.C., Dorman, L.M. & Shen, Y., 1998. Phase velocities of Rayleigh waves in the MELT experiment on the East Pacific Rise, *Science,* **280**(5367), 1235–1238.

Foster, A., Ebinger, C. & Rex, E.M.D., 1997. Tectonic development of the northern Tanzanian sector of the East African Rift System, *J. geol. Soc. Lond.,* **154**(4), 689–700.

Foster, A.N. & Jackson, J.A., 1998. Source parameters of large African earthquakes: implications for crustal rheology and regional kinematics, *Geophys. J. Int.,* **134**(2), 422–448.

Fritz, H., Tenczer, V., Hauzenberger, C., Wallbrecher, E. & Muhongo, S., 2009. Hot granulite nappes—tectonic styles and thermal evolution of the Proterozoic granulite belts in East Africa, *Tectonophysics,* **477**(3–4), 160–173.

Furman, T., Kaleta, K., Bryce, J. & Hanan, B., 2006. Tertiary mafic lavas of Turkana, Kenya: constraints on East African plume structure and the occurrence of high-μ volcanism in Africa, *J. Petrol.,* **47**(6), 1221–1244.

Gao, S. *et al.*, 1997. SKS splitting beneath continental rift zones, *J. geophys. Res.,* **102**(B10), 22 781–22 797.

Goes, S., Govers, R. & Vacher, P., 2000. Shallow mantle temperatures under Europe from P and S wave tomography, *J. geophys. Res.,* **105**(B5), 11 153–11 169.

Green, W.V., Achauer, U. & Meyer, R.P., 1991. A three-dimensional seismic image of the crust and upper mantle beneath the Kenya rift, *Nature,* **354,** 199–203.

Gurnis, M., Mitrovica, J.X., Ritsema, J. & van Heijst, H.-K., 2000. Constraining mantle density structure using geological evidence of surface uplift rates: the case of the African Superplume, *Geochem. Geophys. Geosyst.,* **1**(1), 1020, doi:10.1029/1999GC000035.

Hansen, S.E., Nyblade, A.A. & Benoit, M.H., 2012. Mantle structure beneath Africa and Arabia from adaptively parameterized P-wave tomography: implications for the origin of Cenozoic Afro-Arabian tectonism, *Earth planet. Sci. Lett.,* **319–320,** 23–34.

Huerta, A.D., Nyblade, A.A. & Reusch, A.M., 2009. Mantle transition zone structure beneath Kenya and Tanzania: more evidence for a deep-seated thermal upwelling in the mantle, *Geophys. J. Int.,* **177**(3), 1249–1255.

Johnson, S.P., Waele, B.D. & Liyungu, K.A., 2006. U-Pb sensitive high-resolution ion microprobe (SHRIMP) zircon geochronology of granitoid rocks in eastern Zambia: terrane subdivision of the Mesoproterozoic Southern Irumide Belt, *Tectonics,* **25**(TC6004), doi:10/1029/2006TC001977.

Julià, J., Ammon, C.J., Herrmann, R.B. & Correig, A.M., 2000. Joint inversion of receiver function and surface wave dispersion observations, *Geophys. J. Int.,* **143**(1), 99–112.

Kampunzu, A.B., Bonhomme, M.G. & Kanika, M., 1998. Geochronology of volcanic rocks and evolution of the Cenozoic Western Branch of the East African Rift System, *J. Afr. Earth Sci,* **26**(3), 441–461.

Karato, S. & Karki, B.B., 2001. Origin of lateral variation of seismic wave velocities and density in the deep mantle, *J. geophys. Res.,* **106**(B10), 21 771–21 783.

Kendall, J.M., Stuart, G.W., Ebinger, C.J., Bastow, I.D. & Keir, D., 2005. Magma-assisted rifting in Ethiopia, *Nature,* **433,** 146–148.

Kennett, B.L.N. & Engdahl, E.R., 1991. Traveltimes for global earthquake location and phase identification, *Geophys. J. Int.,* **105**(2), 429–465.

Leggo, P.J., 1974. A geochronological study of the basement complex of Uganda, *J. geol. Soc.,* **130**(3), 263–276.

Lenoir, J.L., Liégeois, J.-P., Theunissen, K. & Klerkx, J., 1994. The Palaeoproterozoic Ubendian shear belt in Tanzania: geochronology and structure, *J. Afr. Earth Sci,* **19**(3), 169–184.

Li, A., 2011. Shear wave model of southern Africa from regional Rayleigh wave tomography with 2-D sensitivity kernels, *Geophys. J. Int.,* **185**(2), 832–844.

Li, A. & Burke, K., 2006. Upper mantle structure of southern Africa from Rayleigh wave tomography, *J. geophys. Res.,* **111**(B10303), doi:10.1029/2006JB004321.

Downloaded from https://academic.oup.com/gji/article-abstract/194/2/961/598895 by guest on 25 September 2018

Li, A., Forsyth, D.W. & Fischer, K.M., 2003. Shear velocity structure and azimuthal anisotropy beneath eastern North America from Rayleigh wave inversion, *J. geophys. Res.,* **108**(B8), 2362, doi:10.1029/2002JB002259.

Lithgow-Bertelloni, C. & Silver, P.G., 1998. Dynamic topography, plate driving forces and the African superswell, *Nature,* **395,** 269–272.

MacDonald, R., Rogers, N., Fitton, G., Black, S. & Smith, M., 2001. Plume-lithosphere interactions in the generation of the basalts of the Kenya Rift, East Africa, *J. Petrol.,* **42**(5), 877–900.

Mana, S., Furman, T., Carr, M.J., Mollel, G.F., Mortlock, R.A., Feigenson, M.D., Turrin, B.D. & Swisher, C.C., III, 2012. Geochronology and geochemistry of the Essimingor volcano: melting of metasomatized lithospheric mantle beneath the North Tanzanian Divergence zone (East African Rift), *Lithos,* (155), 310–325.

McConnell, R.B., 1972. Geological development of the rift system of Eastern Africa, *Geol. soc. Am. Bull,* **83,** 2549–2572.

McConnell, R.B., 1980. A resurgent taphrogenic lineament of Precambrian origin in eastern Africa, *J. geol. Soc. Lond.,* **137,** 483–489.

Mohr, P., 1982. Musings on continental rifts, in *Continental and Oceanic Rifts,* Geodyn. Ser., Vol. 8, pp. 293–309, ed. Palmason, G., AGU, Washington, DC.

Mougenot, D., Recq, M., Virlogeux, P. & Lepvrier, C., 1986. Seaward extension of the East-African Rift, *Nature,* **321,** 599–603.

Mulibo, G.D., 2012. Investigation of mantle structure beneath Eastern Africa: implications for the origin of the Cenozoic tectonism and propagation of the rift system, *PhD thesis,* The Pennsylvania State University.

Mulibo, G.D. & Nyblade, A.A., 2009. The 1994-1995 Manyara and Kwamtoro earthquake swarms: variation in the depth extent of seismicity in northern Tanzania, *South Afr. J. Geol.,* **112,** 387–404.

Mulibo, G.D. & Nyblade, A.A., in press. The P and S wave velocity structure of the mantle beneath eastern Africa and the African superplume anomaly, *Geochem. Geophys. Geosyst*.

Nyblade, A., 2011. The upper mantle low velocity anomaly beneath Ethiopia, Kenya and Tanzania: constraints on the origin of the African Superswell in eastern Africa and plate versus plume models of mantle dynamics, in *Volcanism and Evolution of the African Lithosphere,* pp. 37–50, Geol. Soc. Am. Spec. Publ. 478, Geological Society of America, Boulder, CO.

Nyblade, A.A. & Brazier, R.A., 2002. Precambrian lithospheric controls on the development of the East African rift system, *Geology,* **30,** 755–758.

Nyblade, A.A. & Robinson, S.W., 1994. The African superswell, *Geophys. Res. Lett.,* **21,** 765–768.

Nyblade, A.A., Langston, C.A., Last, R.J., Birt, C. & Owens, T.J., 1996. Seismic experiment reveals rifting of craton in Tanzania, *EOS, Trans. Am. geophys. Un.,* **77**(51), 517–521.

Nyblade, A.A., Owens, T.J., Gurrola, H., Ritsema, J. & Langston, C., 2000. Seismic evidence for a deep upper mantle thermal anomaly beneath East Africa, **28,** 599–602.

Owens, T.J., Nyblade, A.A., Gurrola, H. & Langston, C.A., 2000. Mantle transition zone structure beneath Tanzania, east Africa, *Geophys. Res. Lett.,* **27**(6), 827–830.

Park, Y. & Nyblade, A.A., 2006. P-wave tomography reveals a westward dipping low velocity zone beneath the Kenya Rift, *Geophys. Res. Lett.,* **33**(4), doi:10.1029/2005GL025605.

Park, Y., Nyblade, A.A., Rodgers, A.J. & Al-Amri, A., 2008. S wave velocity structure of the Arabian Shield upper mantle from Rayleigh wave tomography, *Geochem. Geophys. Geosyst.,* **9**(Q07020), doi:10.1029/2007GC001895.

Pasteels, P., Villeneuve, M., Paepe, P.D. & Klerkx, J., 1989. Timing of the volcanism of the southern Kivu province: implications for the evolution of the western branch of the East African Rift system, *Earth planet. Sci. Lett.,* **94**(3–4), 353–363.

Pasyanos, M.E. & Nyblade, A.A., 2007. A top to bottom lithospheric study of Africa and Arabia, *Tectonophysics,* **444,** 27–44.

Priestley, K., McKenzie, D., Debayle, E. & Pilidou, S., 2008. The African upper mantle and its relationship to tectonics and surface geology, *Geophys. J. Int.,* **175**(3), 1108–1126.

Prodehl, C., Fuchs, K. & Mechie, J., 1997. Seismic-refraction studies of the Afro-Arabian rift system—a brief review, *Tectonophysics,* **278,** 1–13.

Ritsema, J., Nyblade, A.A., Owens, T.J., Langston, C.A. & VanDecar, J.C., 1998. Upper mantle seismic velocity structure beneath Tanzania, east Africa: implications for the stability of cratonic lithosphere, *J. geophys. Res.,* **103**(B9), 21 201–21 213.

Ritsema, J., van Heijst, H.K. & Woodhouse, J.H., 1999. Complex shear wave velocity structure imaged beneath Africa and Iceland, *Science,* **286**(5446), 1925–1928.

Roberts, E.M. *et al.*, 2012. Initiation of the western branch of the East African Rift coeval with the eastern branch, *Nature Geosci.,* **5,** 289–294.

Rooney, T.O., Herzberg, C. & Bastow, I.D., 2012. Elevated mantle temperature beneath East Africa, *Geology,* **40**(1), 27–30.

Sebai, A., Stutzmann, E., Montagner, J.-P., Sicilia, D. & Beucler, E., 2006. Anisotropic structure of the African upper mantle from Rayleigh and Love wave tomography, *Phys. Earth planet. Int.,* **155,** 48–62.

Shackelton, R.M., 1986. Precambrian collision tectonics in Africa, in *Collision Tectonics,* pp. 329–349, Geol. Soc. Spec. Publ. 19.

Simmons, N.A., Myers, S.C., Johannesson, G. & Matzel, E., 2012. LLNL-G3Dv3: global P wave tomography model for improved regional and teleseismic travel time prediction, *J. geophys. Res.,* **117**(B10302), doi:10.1029/2012JB009525.

Smith, M.L. & Dahlen, F.A., 1973. The azimuthal dependence of Love and Rayleigh wave propagation in a slightly anisotropic medium, *J. geophys. Res.,* **78,** 3321–3333.

Sobolev, S.V., Zeyen, H., Stoll, G., Werling, F., Altherr, R. & Fuchs, K., 1996. Upper mantle temperatures from teleseismic tomography of French Massif Central including effects of composition, mineral reactions, anharmonicity, anelasticity and partial melt, *Earth planet. Sci. Lett.,* **139,** 147–163.

Stamps, D.S., Calais, E., Saria, E., Hartnady, C., Nocquet, J.M., Ebinger, C.J. & Fernandes, R.M., 2008. A kinematic model for the East African Rift, *Geophys. Res. Lett.,* **35**(L05304), doi:10.1029/2007GL032781.

Sykes, L.R. & Landisman, M., 1974. The seismicity of East Africa, the Gulf of Aden and the Arabian and Red Seas, *Bull. seism. Soc. Am.,* **54,** 1927–1940.

Tugume, F., Nyblade, A. & Julià, J., 2012. Moho depths and Poisson's ratios of Precambrian crust in East Africa: evidence for similarities in Archean and Proterozoic crustal structure, *Earth planet. Sci. Lett.,* **355–356,** 73–81.

Venkataraman, A., Nyblade, A.A. & Ritsema, J., 2004. Upper mantle Q and thermal structure beneath Tanzania, East Africa from teleseismic P wave spectra, *Geophys. Res. Lett.,* **31**(L15611), doi:10.1029/2004GL020351.

Vinnik, L.P., Makeyeva, L.I., Milev, A. & Usenko, A.Y., 1992. Global patterns of azimuthal anisotropy and deformations in the continental mantle, *Geophys. J. Int.,* **111**(3), 433–447.

Walker, K.T., Nyblade, A.A., Klemperer, S.L., Bokelmann, G.H.R. & Owens, T.J., 1994. On the relationship between extension and anisotropy: constraints from shear wave splitting across the East African Plateau, *J. geophys. Res.,* **109**(B08302), doi:10.1029/2003JB002866.

Weeraratne, D.S., Forsyth, D.W., Fischer, K.M. & Nyblade, A.A., 2003. Evidence for an upper mantle plume beneath the Tanzanian craton from Rayleigh wave tomography, *J. geophys. Res.,* **108,** 2427, doi:10.1029/2002JB002273.

Wessel, P. & Smith, W.H.F., 1998. New, improved version of the Generic Mapping Tools released, *EOS, Trans. Am. geophys. Un.,* **79,** 579.

Wiens, D.A., Conder, J.A. & Faul, U., 2008. The seismic structure and dynamics of the mantle wedge, *Annu. Rev. Earth planet. Sci.,* **36,** 421–455.

Wohlenberg, J., 1969. Remarks on the seismicity of east Africa between 42N-12S and 23E-40E, *Tectonophysics,* **8**(4–6), 567–577.

Yang, Y. & Forsyth, D.W., 2006a. Regional tomographic inversion of the amplitude and phase of Rayleigh waves with 2-D sensitivity kernels, *Geophys. J. Int.,* **166,** 1148–1160.

Yang, Y. & Forsyth, D.W., 2006b. Rayleigh wave phase velocities, small-scale convection, and azimuthal anisotropy beneath southern California, *J. geophys. Res.,* **111**(B07306), doi:10.1029/2005JB004180.

Zhou, Y., Dahlen, F. & Nolet, G., 2004. Three dimensional sensitivity kernels for surface wave observables, *Geophys. J. Int.,* **158,** 142–168.

Downloaded from https://academic.oup.com/gji/article-abstract/194/2/961/598895 by guest on 25 September 2018